Check for updates

Lab-on-a-chip models of the blood–brain barrier: evolution, problems, perspectives

Mária A. Deli, [iD] *[a] Gergő Porkoláb, [iD] [ab] András Kincses,[a] Mária Mészáros,[a] Anikó Szecskó, [iD] [ab] Anna E. Kocsis,[a] Judit P. Vigh,[ab] Sándor Valkai,[a] Szilvia Veszelka,[a] Fruzsina R. Walter [iD] [a] and András Dér [iD] [a]

A great progress has been made in the development and use of lab-on-a-chip devices to model and study the blood–brain barrier (BBB) in the last decade. We present the main types of BBB-on-chip models and their use for the investigation of BBB physiology, drug and nanoparticle transport, toxicology and pathology. The selection of the appropriate cell types to be integrated into BBB-on-chip devices is discussed, as this greatly impacts the physiological relevance and translatability of findings. We identify knowledge gaps, neglected engineering and cell biological aspects and point out problems and contradictions in the literature of BBB-on-chip models, and suggest areas for further studies to progress this highly interdisciplinary field. BBB-on-chip models have an exceptional potential as predictive tools and alternatives of animal experiments in basic and preclinical research. To exploit the full potential of this technique expertise from materials science, bioengineering as well as stem cell and vascular/BBB biology is necessary. There is a need for better integration of these diverse disciplines that can only be achieved by setting clear parameters for characterizing both the chip and the BBB model parts technically and functionally.

[a] HUN-REN Biological Research Centre, Institute of Biophysics, Szeged, Hungary.
E-mail: deli.maria@brc.hu
[b] Doctoral School of Biology, University of Szeged, Hungary

1. Introduction

The importance of the blood–brain barrier (BBB) in biomedical sciences is undisputable. The proper function of cerebral capillaries forming the BBB is one of the key factors in the maintenance of brain homeostasis, while BBB

Mária Deli

Prof. Mária Deli received her MD and PhD degrees from the University of Szeged and her DSc degree from the Hungarian Academy of Sciences. She is a Research Professor and Head of the Biological Barriers Research Group at HUN-REN Biological Research Centre, Institute of Biophysics in Szeged, Hungary. She pioneered novel complex co-culture models of the blood–brain and different epithelial barriers. Her research interests include barrier models in lab-on-a-chip devices; organ-on-chip models; barrier dysfunction and protection in diseases; drug and targeted nanoparticle delivery across biological barriers.

András Dér

Prof. András Dér received his MSc degree in physics (1980) and PhD degree in computer science (1988) from József Attila University, Szeged, and DSc degree from the Hungarian Academy of Sciences (1999). He had been the Deputy Director of the Institute of Biophysics, Biological Research Centre; and the Vice President of the Hungarian Biophysical Society. He is a Scientific Advisor and Head of the Biomolecular Electronics Research Group at the HUN-REN Biological Research Centre, Institute of Biophysics. He is co-inventor of several patents about lab-on-a-chip applications in bioelectronics and medicine. His major research interests include protein dynamics, biophotonics, and bioelectronics.

dysfunction is linked to many acute and chronic neurological diseases,[1] as well as to systemic inflammatory conditions. Given the fundamental role of the BBB in drug and nanoparticle transport to the central nervous system, there is a growing interest in the development and use of complex models mimicking the human BBB. The first BBB-on-chip model, a lab-on-a-chip (LOC) device incorporating brain endothelial cells was described 12 years ago[2] (Fig. 1),[2–16] and since then more than 150 papers have been published on microfluidic chip devices and the BBB. Importantly, all these models are based on cultured cells of the BBB.

To give a perspective on the evolution of BBB-on-chip systems, the first pioneering work on culture models of the BBB was reported 45 years ago (Fig. 1).[2–16] Culture models are widely used and valuable tools in basic and preclinical research to study the cellular and molecular aspects of BBB physiology, pharmacology and pathology.[17,18] Following the first observation that endothelial cells grow out from isolated rat cerebral capillaries in sterile culture conditions[7] many advancements have been made in this field (Fig. 1).[2–16] One of the major milestones was the introduction of culture inserts containing porous membranes to grow primary brain endothelial monolayers.[8] This was the first BBB model with two fluid compartments, mimicking the vascular and brain sides, to allow permeability assays and later the

measurement of transendothelial electrical resistance (TEER). Since primary brain endothelial cells easily lose their unique phenotype when kept in mono-culture, especially after more than two passages, in the next generation of BBB models brain endothelial cells were kept in co-culture with glial cells,[9,10] then with astrocytes and brain pericytes.[11,12] Another major improvement in the field was the development of human BBB models using brain-like endothelial cells differentiated from induced pluripotent stem cells (iPSCs)[13] or hematopoietic stem cells derived from umbilical cord blood.[14] However, these models have limitations. To ensure both the vascular endothelial identity and BBB properties of iPSC-derived cells a two-step differentiation protocol was described.[15] Finally, to enhance the weak barrier and other BBB characteristics of iPSC-derived human models differentiated from endothelial progenitors, a new method was invented simultaneously targeting multiple signaling pathways using small molecules.[16] The long-term goal is to create human body-on-chip systems with integrated BBB-on-chips for biomedical research including disease modeling, drug discovery and personalized medicine.[19]

In this review we present the main types of BBB-on-chip models and their use for the investigation of certain aspects of BBB physiology, drug and nanoparticle transport, toxicology and selected areas of pathology. Due to significant
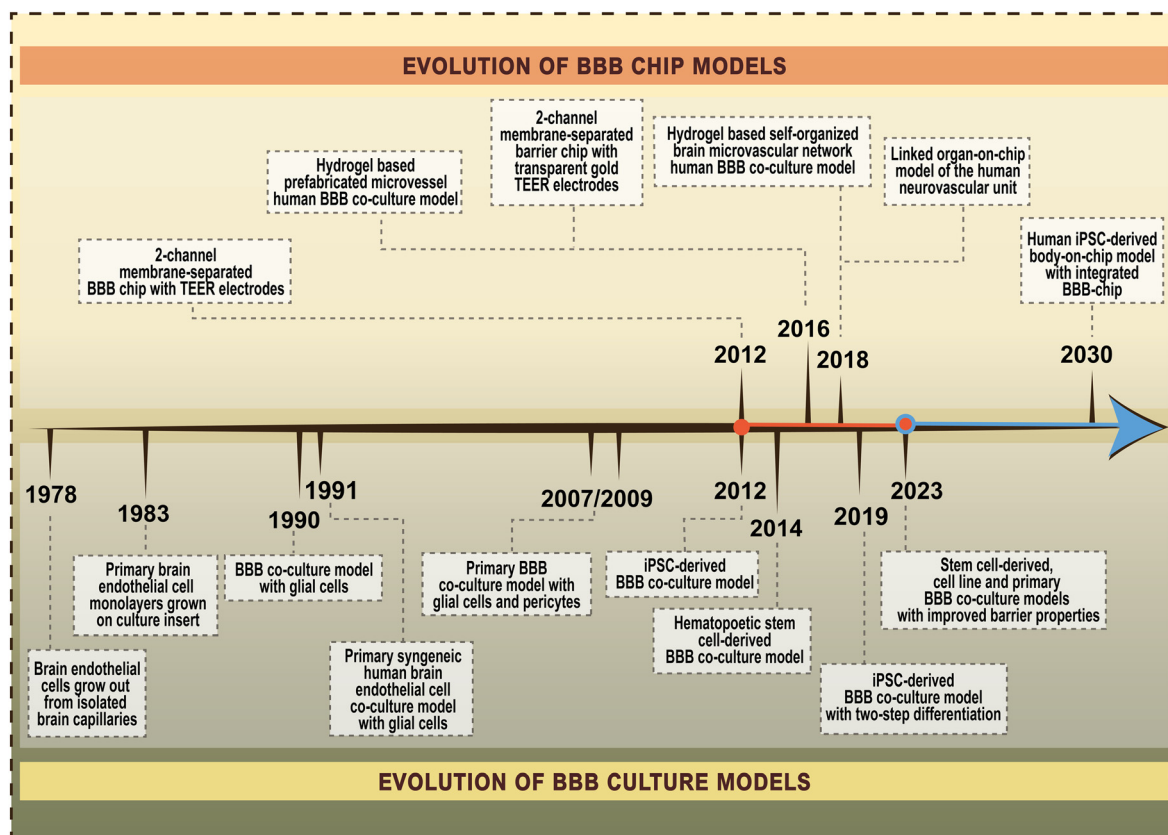

Fig. 1 Timeline of the evolution of blood–brain barrier (BBB) chip models and BBB culture models. References for the selected major milestones of BBB chip models in order of publication time.[2–6] References for the selected major milestones of BBB culture models in order of publication time.[7–16]

differences between cerebral and peripheral endothelial cells on many levels, only BBB-on-chip devices with brain endothelial cells are discussed. Our main goals are to identify knowledge gaps, neglected engineering and cell biological aspects, to point out problems and contradictions in the literature of BBB-on-chip models, and to suggest areas for further studies to progress this highly interdisciplinary field.

2. Evolution of LOC devices to study the BBB

LOC devices became more and more popular tools for barrier studies in the last decade (Fig. 1).[2–16] The channels and sensors provide better opportunities to model the physiological conditions *in vitro*.[20] The small size of LOC tools makes it easy to transport them between the CO_2 incubator and the measurement devices, or even enables to perform the measurements inside the incubator. BBB studies especially profited from the breakthrough of the LOC techniques, since the dynamic LOC devices have several advantages compared to static culture inserts, *e.g.* closed and well-defined channels, three-dimensional cell-cultures, integrated electrodes or attachable pumps for medium exchange/constant fluid flow. The first LOC devices with on-chip sensors/assays using a BBB co-culture model were published in 2012.[2,21] These studies represented the first main path of BBB-on-chip evolution for the following decade. The common characteristics of these devices were the solid, porous supports providing cell-culture surfaces for the different cell types which had no direct contact with each
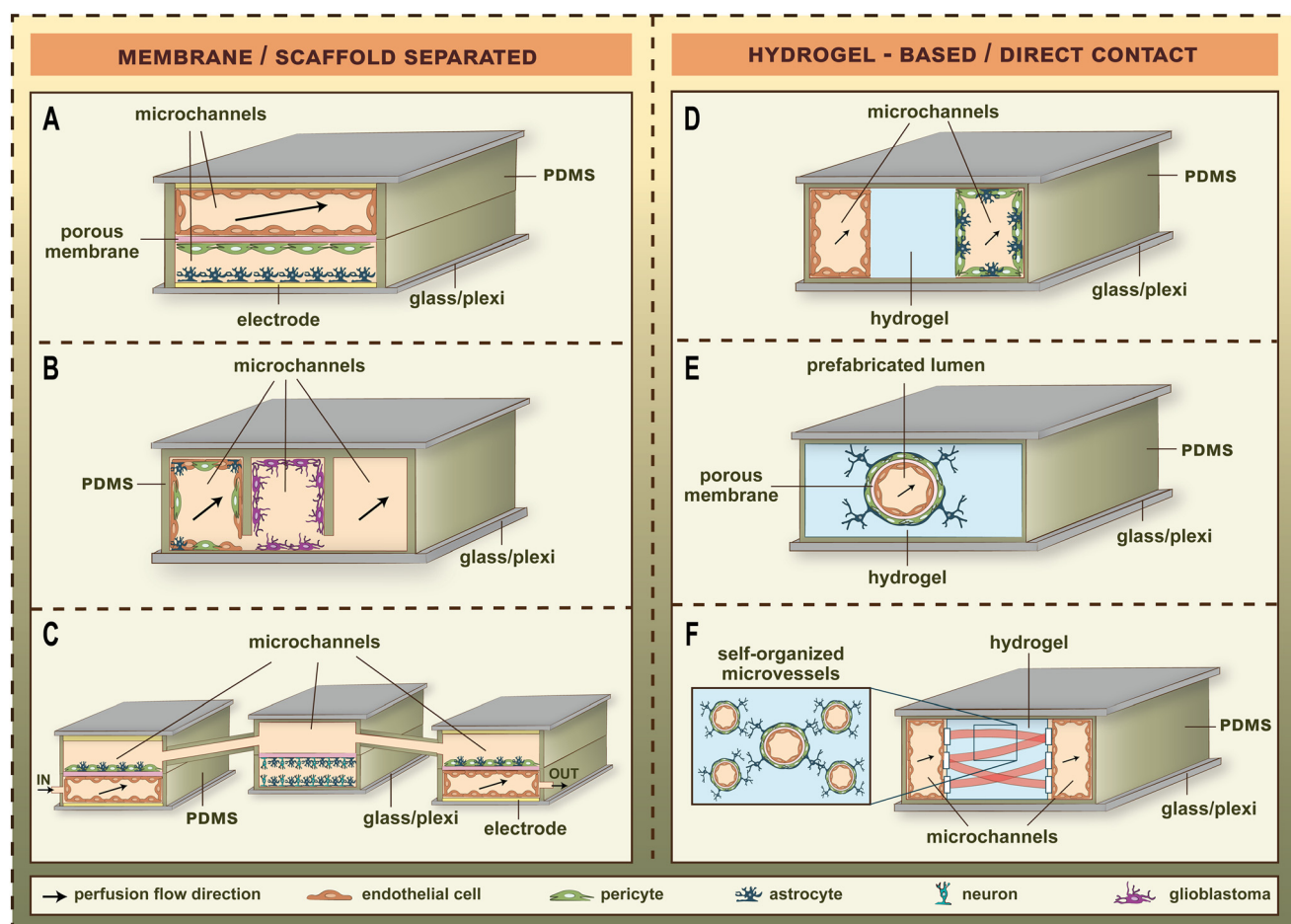

Fig. 2 The major types of blood–brain barrier (BBB) chip models. (A) Dual-channel membrane-separated chip from polydimethylsiloxane (PDMS) with transparent gold electrodes to measure transendothelial electrical resistance.[4] (B) Three-lane scaffold-separated chip from *in situ* functionalized PDMS with two microfluidic channels for the measurement of drug permeability.[22] (C) Neurovascular organ-on-chip consisting of three connected microfluidic chips named influx BBB chip, brain chip, efflux BBB chip. Each chip contains two channels separated by porous membranes. The vascular microchannels of the BBB chips contain electrodes for resistance measurement and are perfused with culture medium.[6] (D) Three-lane dual-channel hydrogel-based microfluidic chip in multiwell plate format. The vascular microchannel covered by brain endothelial cells and the second microchannel containing astrocytes and brain pericytes are perfused with culture medium, and separated by a hydrogel in the middle.[23] (E) Single-channel hydrogel-based microfluidic chip with predefined tubular hydrogel template.[3] (F) Hydrogel-based self-organized brain microvascular network in a PDMS-based device with three parallel compartments separated by posts. The central hydrogel compartment is flanked by two flow channels. The medium channels are covered by brain endothelial cells, and the fibrin hydrogel contains brain endothelial, astrocyte and brain pericyte cells to study vasculo- and angiogenesis.[5]

other (Fig. 2).[3–6,22,23] Most of these devices contain a porous plastic membrane, which is also separating the culture channels, while some of them apply porous scaffolds built up using microfabrication techniques. The other main group of BBB-on-chip devices (Fig. 2)[3–6,22,23] enables direct contact between the different cell types. In this case, the capillary channels are formed in hydrogels, and the pericytes, astrocytes or other neurovascular cell types are embedded in the gel. The two types of chip devices have different advantages, discussed in the following paragraphs (Table 1).[2–6,21,24–37]

2.1 LOC devices with membrane or scaffold-separated channels

These LOC devices generally consist of a top and bottom channel, which are separated by the porous cell culture membrane. This geometry enables transendothelial electrical resistance (TEER) measurements with quasi-direct current (DC) or electrical impedance spectroscopic methods, permeability assays and constant monitoring of the cells *via* phase contrast microscopy. Examples of TEER, as well as combined TEER and streaming potential measurements on BBB-on-chips are shown in Fig. 3.[2,4,31,34]

The first representatives of these devices were built up by a pair of perpendicularly overlapping channels separated by a polycarbonate porous membrane, and flow was applied in the top/vascular channel for dynamic modeling of the BBB.[2,24] Booth *et al.*[25] designed a 4-point measurement setup for the determination of TEER. The endothelial cells were cultured on the membrane in the top channel, and the astrocytes in the top side of the bottom channel, forming a vertically layered co-culture (Fig. 2).[3–6,22,23] The two pairs of AgCl electrodes were located above and below the cell culture membrane (Fig. 3), in a geometry that resulted in a uniform distribution of the ion flow. The integrated electrodes were formed on glass slides with sputter coating and chlorination. The TEER measurement was carried out using the commercially available and widely used EVOM2 Voltohmmeter (World Precision Instruments, Sarasota, FL, USA), which applied a 10-µA amplitude square-wave signal at 12.5 Hz frequency, and measured the resistance: TEER = $(R_c - R_b)A$, where R_c and R_b stand for the total and background resistance, respectively, and A is the area of the membrane. This LOC device was also suitable for performing permeability assays.

Griep *et al.*[24] took a different approach for the electrical measurements. Instead of the quasi-DC method (EVOM2), they chose to measure the electrical impedance spectrum *via* a pair of platinum wires placed in extra channels close to the overlapping cell-culture region containing the endothelial monoculture. The resistance values were calculated using the least-square fitting method on the equivalent circuit model.[38] In both cases the cells were visualized *via* immunocytochemistry.

Table 1 The major types of chip devices and their parameters to model the blood–brain barrier[2–6,21,24–37]

Year	Surface material	Surface geometry	Channel/compartment	Permeability markers	TEER/EIS	Sensors	Microscopy	Ref.
Membrane or scaffold separated channels								
2012	Polycarbonate	Porous membrane	Two perpendicular channels	FITC–dextran 4, 20, 70 kDa	TEER (EVOM2)	—	Fluorescence microscopy	2
2013	PDMS	Channels with walls with microchannels	Two sidechannels and a central compartment	FITC–dextran 4 kDa	—	—	Phase contrast and fluorescence microscopy	21
2013	Polycarbonate	Porous membrane	Two perpendicular channels	—	EIS	—	Confocal microscopy	24
2014	Polycarbonate	Porous membrane	Two perpendicular channels	FITC–dextran 4 kDa, propidium iodide	TEER (4-point measurement)	Integrated microflow sensor – wall shear stress	Fluorescence microscopy	25
2015	PTFE/PE	Porous membrane	Two parallel channels	FITC–dextran 70 kDa	—	—	Phase contrast microscopy	26
2016	Polycarbonate	Porous membrane	Two parallel channels	FITC–dextran 10 kDa	TEER	—	Fluorescence microscopy	27
2016	Polycarbonate	Porous membrane	Two parallel channels	—	TEER	—	Phase contrast and fluorescence microscopy	28
2016	Polycarbonate	Porous membrane	Two perpendicular main channels, additional sidechannel network	Fluorescein, FITC–dextran 70 kDa	—	—	Fluorescence microscopy	29
2016	PET	Porous membrane	Two parallel channels	Fluorescein, FITC–dextran 4 kDa, Evans blue–albumin	TEER (EVOM2)	—	Phase contrast and confocal microscopy	4
2018	PET	Porous membrane	Two parallel channels, 3 chips	Cascade blue, albumin	—	—	Confocal microscopy	6

Table 1 (continued)

Year	Surface material	Surface geometry	Channel/compartment	Permeability markers	TEER/EIS	Sensors	Microscopy	Ref.
Membrane or scaffold separated channels			connected in-line					
2019	NPN	Porous membrane	Two perpendicular channels	Lucifer yellow	—	—	Phase contrast and transmitted light microscopy	30
2020	PET	Porous membrane	Two parallel channels	FITC–dextran 10 kDa	TEER	—	Phase contrast and confocal microscopy	31
2020	—	Porous membrane	Two parallel channels, two additional flanking channels for the bottom channel	FITC–dextran 4, 40 kDa	TEER	—	Transmission electron and confocal microscopy	32
2023	NPN	Porous membrane	Two parallel channels	—	—	Digital sensor patches for cytokines/chemokines	Fluorescence and confocal microscopy	33
Hydrogel-based models								
2016	Collagen	Cylindrical tube	Single channel	Alexa488-dextran 3 kDa	—	—	Bright-field and confocal microscopy	3
2017	Hydrogel	Cylindrical channels	Two parallel channels, connection through gel compartment	FITC–dextran 4 kDa	EIS, TEER	—	Inverted epifluorescence, confocal and transmission electron microscopy	34
2018	Glass and polymers	Rectangular channels	Two-lane and tree-lane chips with hydrogel in multiwell format	FITC–dextran 20 kDa	—	—	Confocal microscopy	35
2018	Glass and PDMS	Rectangular channels	Central gel channel with two adjacent medium channels	FITC–dextran 10 and 40 kDa for perfusion	—	—	Phase contrast and confocal microscopy	5
2021	Polymer	Rectangular channels	Central gel channel with two adjacent medium channels	Texas red 594-dextran 70 kDa	—	—	Confocal microscopy	36
2022	PDMS	Rectangular channels	Central gel channel and two adjacent medium channels	FITC–dextran 10, 40, 150 kDa	—	—	Confocal and scanning electron microscopy	37

Abbreviations: EIS, electric impedance spectroscopy; EVOM2, epithelial voltohmmeter (World Precision Instruments); FITC, fluorescein isothiocyanate; NPN, nanoporous silicon nitride; PDMS, polydimethylsiloxane; PE, polyethylene; PET, polyester; PTFE, polytetrafluoroethylene; TEER, transendothelial electrical resistance.

Fig. 3 Examples of electrode placement, and measurement of TEER as well as combined TEER and streaming potential in BBB-on-chip devices.[2,4,31,34] Current electrodes are shown in red, whereas voltage electrodes are shown in blue color.

Prabhakarpandian *et al.*[21] reported the first channel system with porous walls as cell-support. The two 200-μm wide side channels were connected to a large central compartment through 50-μm long and 3-μm wide channels. The brain endothelial cells and astrocytes were cultured in the side channels where the cells grew on the walls, as well. The integrity of the BBB was evaluated *via* FITC–dextran permeability measurements. The visualization of the cells was limited to the bottom side of the channels, and was performed with phase-contrast microscopy and fluorescent imaging.[21]

Sellgren *et al.*[26] reported the first BBB-on-chip LOC device with parallel channels separated by a polytetrafluoroethylene (PTFE) membrane. Brain endothelial cells were cultured in the top channel, and astrocytes in hydrogel were seeded in the bottom channel. A great advantage of the device was that the cells could be visualized with optical microscopy.[26] The BBB integrity was evaluated by permeability assays, and the morphology of the cells was visualized with immunocytochemistry.[26] Brown *et al.*[27] reported a LOC device with similar structure: brain endothelial cells were cultured in the top compartment on a polycarbonate porous membrane, while astrocytes and brain pericytes on the bottom side of the membrane, and the lower compartment was loaded with collagen gel containing stem-cell-derived neurons and astrocytes.[27] This complex neurovascular unit was used for investigating the BBB effects of inflammatory signals using different stimulations. TEER and immunocytochemistry were performed on-chip, while ELISA and mass spectrometric investigation of metabolites were tested off-chip.[27]

Most of the devices focus on a few special features. However, Walter *et al.*[4] published a versatile LOC tool, which allowed the co-culture of several cell types and the flow of culture medium and was able to monitor all the crucial barrier parameters of the BBB, such as visualization of the entire endothelial cell layer by microscopy, TEER measurement in real-time and permeability assays. The device had two parallel channels, with the possibility of constant fluid flow for the dynamic experiments. This device was tested for several different biological barrier models.[4] In case of the BBB models, brain endothelial cells were seeded in the top channel, and for the co-culture brain pericytes were cultured on the bottom side of the membrane, and glial cells at the bottom of the lower channel. The TEER was measured with an EVOM2 device using 25-nm thick transparent gold electrodes (Fig. 3), which covered uniformly the entire area of the brain endothelial monolayer.[4] The cells could be monitored *via* phase contrast microscopy during the whole experiment. Permeability assays and immunohistochemistry were also performed.[4] An improved version of the device was equipped with a pair of Ag/AgCl electrodes at the inlet/outlet of the flow channel (Fig. 3) making it possible to evaluate the surface-charge properties of the confluent brain endothelial monolayer.[31]

After the first period of LOC device development, where the main focus was to create functional devices to investigate the basic barrier properties of the BBB, the focus shifted toward more specific applications, involving various analytical techniques. Ahn *et al.*[32] reported a drug delivery study in a LOC device mimicking the physiological structure of the brain. An endothelial flow channel and a bottom channel with hydrogel-embedded pericytic-astrocytic network enabled TEER measurement, nanoparticle sampling, and fluorescence-activated cell sorting (FACS) analysis under physiological-like and pathological conditions mimicking inflammation.[32] Metabolic sensors have huge potential, however the inclusion of such sensors in the micrometer scale might be challenging. Su *et al.*[33] published a device with three digital sensor patches for cytokines/chemokines at

the abluminal side. Great advantage of the device is that the inflammatory factors are measured on-chip.

2.2 Hydrogel-based LOC models

The other group of the BBB-on-chip devices focuses on the recapitulation of the physiological structure of the brain capillaries (Fig. 2).[3–6,22,23] In these models permeability assays by imaging techniques are applied to evaluate barrier integrity. Herland *et al.* published the first device with a cylindrical channel formed in collagen gel to study the BBB.[3] The gel was embedded in a polydimethylsiloxane (PDMS)-based chip, and the channel was created *via* the so-called "viscous fingering" method. The application of hydrostatically controlled medium tunneled the viscous collagen solution, which was then incubated under 37 °C, to promote gelation.[3] Brain endothelial cells and the pericytes were cultured on the gel surface, while the astrocytes were embedded in the gel. The geometry does not allow TEER measurement, thus the paracellular permeability was evaluated using 3 kDa dextran. The cells were visualized with fluorescent imaging.[3] Partyka *et al.*[34] prepared two parallel cylindrical channels, which were connected through a chamber filled with hydrogel. The channels were formed with the insertion of two acupuncture needles before polymerization, which were removed after the hydrogel became rigid. The endothelial cells were seeded in one of the channels, the astrocytes were embedded in the hydrogel.[34] TEER was measured *via* electric impedance spectroscopy (EIS) with a pair of electrodes placed in each channel's inlet port (Fig. 3), and the paracellular permeability was evaluated by the transfer of 2 kDa dextran from the endothelial channel through the hydrogel to the medium channel. The cells were visualized using bright-field microscopy and immunocytochemistry.[34]

LOC devices in BBB studies hold great potential in drug discovery and drug delivery, but high-throughput is a key factor for successful implementation. Two-lane and tree-lane chips with hydrogel in multi-well plate format are potential candidates for the task, as these systems are commercially available. Wevers *et al.*[35] presented mono- and co-culture BBB models in the two-lane and three-lane versions, respectively. The lanes are not physically separated, but small ribs called phaseguides provide the separation. The phaseguides act as meniscus pinning barriers keeping the fluids/gel in the lanes.[35] The two-lane configuration was used for a mono-culture, while the three-lane version was used for a co-culture model. In the case of the mono-culture, one of the two lanes was filled with gel, while the other one with the brain endothelial cells. The co-culture model's middle channel was filled with the gel, the first channel was seeded with the brain endothelial cells, and the third channel with the astrocytes and brain pericytes.[35] A gravity-driven leveling technology provided the perfusion in the channels, resulting a periodically changing flow-direction. The barrier integrity was assessed *via* fluorescent imaging and antibody

transcytosis. Both configurations allow high-throughput screening, since the two-lane and three-lane chip plates are available in 96-chip per plate and 40- or 64-chip per plate configurations, respectively.[35]

To understand the processes of vascularization and angiogenesis is fundamental for basic research and applied sciences, like tissue engineering. LOC applications with self-organizing microvascular networks are useful tools for these studies. Campisi *et al.*[5] reported the first PDMS-based device with three parallel compartments separated by posts. The central hydrogel channel was flanked by two medium/flow channels (Fig. 2). The medium channels were covered by brain endothelial cells and the fibrin hydrogel contained brain endothelial, astrocyte and pericyte cells and also factors to promote angiogenesis and vascularization.[5] The integrity of the vascular network was evaluated by the analysis of immunocytochemistry images. The gene expression experiments were carried out with RT-PRC tests. Perfusability was tested with fluorescent tracers (FITC–dextran).[5] The bulk flow of interstitial fluid plays an important role in the development of the microvascular network. Winkelman *et al.*[36] introduced a method to evaluate the effects of the interstitial flow on self-organizing brain microvascular networks in a microfluidic device. The flow through the hydrogel was due to the applied pressure difference between the flow channels. The dynamic conditions were beneficial for both angiogenesis and vasculogenesis, compared to the static version of the setup: enhanced vessel area, branch length, diameter, connectivity and longevity were detected.[36] The barrier integrity was evaluated by dextran permeability, which also showed lower values in the case of dynamic conditions. The cells were visualized with fluorescent microscopy, and protein immunofluorescent assays were performed to evaluate the expression of basal lamina proteins.[36]

2.3 Problems and perspectives

As a general tendency, the evolution of biochips points toward having increased integration and number of elements on them, to be able to model various features of biological structural units, and to perform more cost-effective and faster experiments. Given the present-day technology, however, the functional complexity of the BBB does not allow to model all features, and integrate all types of sensors on a single chip. Hence, the actual implementations of BBB chip models are adapted to the certain physiological problems aimed to address. As for the basic architecture of BBB chips, both the porous-membrane-based and the gel-based structures (Fig. 2)[3–6,22,23] have their scopes of application, which is expected to hold on in the near future, too.

In spite of the recent progress in microfabrication methods, the integration of various sensors on a single chip remains a significant challenge, mainly due to the limited space and the potential interference between different sensing components.[9] To address these issues, it appears

necessary to physically separate different monitoring functions.[20]

For real-time assessment of crucial physical parameters, however, direct access to the BBB model is essential. It is achieved using electrical sensors that measure TEER and/or zeta-potential to gauge transmembrane conductivity and surface electric charge (Fig. 3), respectively.[39] Where possible, imaging techniques like phase-contrast or fluorescent microscopy, should also be employed for the continuous monitoring of the growth of the cells on the culture surface, and for the validation of the proper, confluent brain endothelial cell layer in the biochip,[4,40] A new BBB-on-chip model by Wei *et al.* integrated barrier monitoring by TEER measurement and fluorescence microscopy in real time.[41]

On the other hand, the monitoring of chemical and biochemical signals can be accomplished at separate locations, with connections to the primary BBB module through microfluidic channels.[29,42] It is anticipated, therefore, that we will soon see the creation of modular networks consisting of microfluidic BBB chip and biosensor systems, which will have a wide range of applications in both fundamental, scientific research and practical use. These networks will incorporate online control and measurement tools to generate a series of data over time, each containing distinct information related to barrier properties. To effectively analyze these intricate data sets, artificial intelligence techniques are expected to offer significant advantages.[43,44] These advanced platforms will provide pronounced adaptability and versatility for conducting scientific studies on BBB culture models. Additionally, they will be readily combined with other platforms employing *e.g.*

brain, epithelial and/or lung organoids, towards even more complex body-on-a-chip platforms. These advanced lab-on-a-chip systems hold great promise for specific applications in point-of-care diagnostics, as well.

3. Types of brain endothelial cells used in LOC devices to model the BBB

Besides choosing the right geometry, it is also important to select the appropriate cell types to be integrated into BBB-on-chip devices, as this will greatly impact the physiological relevance and translatability of findings. The term BBB refers to the unique anatomical and functional properties of brain microvascular endothelial cells compared to blood vessels in the periphery. Therefore, the main cell type of BBB-on-chip devices are brain endothelial cells. Brain endothelial cells commonly used in BBB-on-chip devices can be divided into three broad categories depending on the source of cells: i) immortalized brain endothelial cell lines, ii) primary brain endothelial cells and iii) stem cell-derived brain-like endothelial cells (Fig. 4). Although human umbilical vein endothelial cells (HUVECs) have been reported as a BBB model before, these are general vascular endothelial cells that do not possess brain endothelial characteristics and accordingly, it will not be discussed here.

3.1 Brain endothelial cell lines

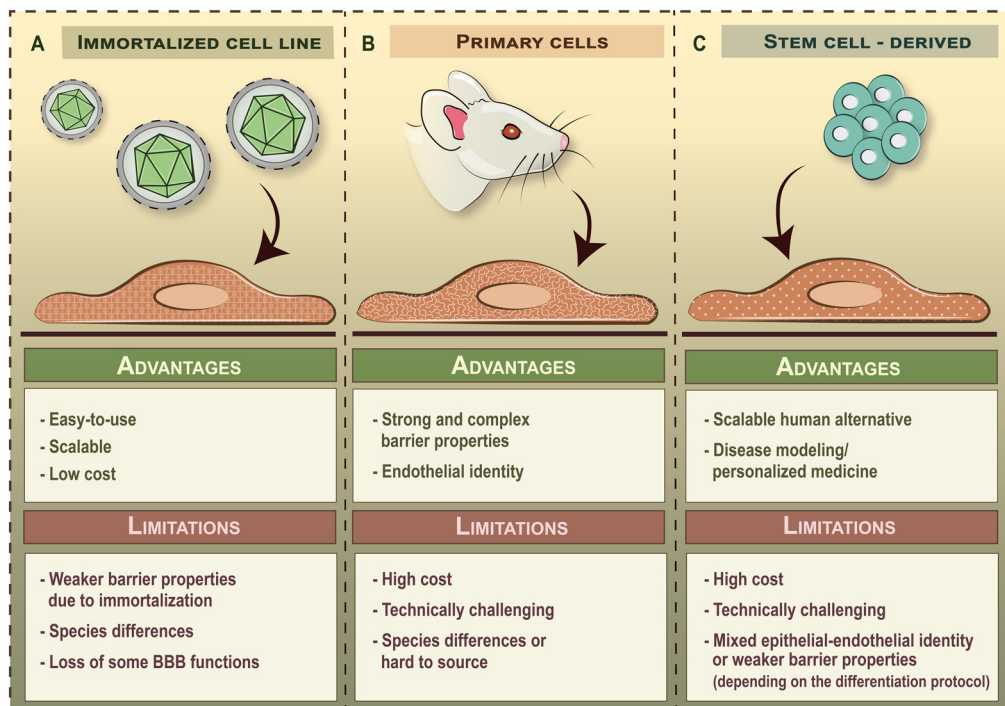Commercially available brain endothelial cell lines are derived from animal- or human tissue. To overcome cellular

Fig. 4 The three major types of brain endothelial cells used in blood–brain barrier chip models.

senescence in culture, these cells are immortalized by transduction of telomerase subunits or tumor antigens using lenti- or retroviruses. As a result, immortalized brain endothelial cell lines grow rapidly and can be used for several but limited passages (*e.g.* ≤35 passages for hCMEC/ D3 line) in culture,[45] which makes them a readily available candidate for modeling the BBB. Indeed, brain endothelial cell lines were among the first cells to be integrated into BBB-on-chip devices and are still widely used today. Popular brain endothelial cell lines cultured under dynamic flow conditions include the mouse bEnd.3 (ref. 2, 25, 26, 46 and 47) and cerebEND lines,[48] the rat RBE4 line,[21,48] as well as human hCMEC/D3,[4,22,24,28,29,50–54] TY10,[35] and HBMEC-IM[32] cell lines (Table 2).[2–6,21–30,32,33,35,37,40,46–67] Although the easy-to-use nature of brain endothelial cell lines is favorable from a practical point of view, these cells have several limitations (Fig. 4A) and non-physiological characteristics due their viral immortalization. Brain endothelial cell lines typically have weak paracellular barrier properties and a lower activity of efflux pumps compared to other cellular sources.[68]

3.2 Primary brain endothelial cells

Primary brain endothelial cells are also isolated from animal- or human tissue but are not immortalized. Consequently, these cells have higher paracellular barrier tightness and appropriate transporter activity and polarity (Fig. 4B). This, in theory, would make primary brain endothelial cells the ideal candidates for modeling the BBB. However, these cells gradually lose their BBB phenotype upon subculturing,[69] and therefore, can only be used at low passage numbers (≤2). Added to this, the isolation and maintenance of primary brain endothelial cells requires special technical skills and offers a relatively inflexible timeline for experiments. Indeed, primary brain endothelial cells have been less commonly integrated into BBB-on-chip devices then brain endothelial cell lines so far[3,4,6,23,27,33,37,55] (Table 2). Another important aspect that has to be addressed is the presence of major interspecies differences at the BBB,[70–73] especially in the level of proteins involved in drug transport, which negatively impacts the translatability of findings from animal cell-based models to human clinical trials. An optimal solution for this problem would be to use freshly isolated primary brain endothelial cells from human or non-human primate tissue,[74] but these cells have limited availability and their use has to meet rigorous ethical requirements. Although primary human brain endothelial cells are commercially available, these cells have already been subcultured before cryopreservation (generally shipped between passage 1–5), which greatly limits their further usability and their capacity to be expanded in culture.

3.3 Stem cell-derived brain-like endothelial cells

Brain-like endothelial cells differentiated from human stem cells represent the state-of-the-art of human *in vitro* BBB models as stem cell lines are readily available, have good

scalability and can be used for disease modeling when derived from patients (Fig. 4C). In the past decade, several laboratories established human stem cell-derived BBB models, differentiated from iPSCs[13,15,75–84] or CD34^{+} hematopoietic stem cells derived from umbilical cord blood.[14,85,86] As this technology advances in parallel with LOC engineering, stem cell-derived brain-like endothelial cells are more commonly getting integrated into BBB-on-chip devices[5,30,40,53,56–67] (Table 2). However, the field remains highly controversial as the method of differentiation greatly impacts the identity of cells.[87–89] Therefore, care should be taken when selecting brain-like endothelial cell differentiation protocols and interpreting results from these studies.

Currently used stem cell-derived brain-like endothelial cells can be further divided into two main groups based on their cellular identity. The first group features models that have an extremely high paracellular barrier tightness but possess a mixed epithelial–endothelial character that resembles those of neuroectodermal epithelial cells. Corresponding differentiation protocols generally take less than 14 days to perform and include the addition of retinoic acid during a specification step towards the brain-like phenotype.[90] Such BBB models are generally referred to as iBMECs. Although iBMECs form a tight barrier, they suffer from the lack of a definitive vascular character, which is a major limitation when studying drug transport or immune cell trafficking.[83] On the other end of the spectrum are models that possess a definitive vascular character but have weak paracellular barrier properties. Corresponding protocols include a two-step differentiation process, in which stem cells are first differentiated into vascular endothelial progenitors through mesoderm induction and BBB-like characteristics are induced as a second step, without the addition of retinoic acid. Such BBB models include those using CD34^{+} hematopoietic stem cells derived from umbilical cord blood,[14,85,86] as well as the newest generation of iPSC-derived brain-like endothelial cells,[15,83,84] which have also been integrated into BBB-on-chip devices.[30,40,53,56] The major limitation of the second group of cells is their leakier barrier phenotype as compared to primary cell-based models (Table 2), which has to be strengthened in order to assess drug penetration in a reliable way. In either case, the applicability of these models is limited to specific applications, which highlights the need to better mimic both the endothelial nature and the complexity of the human BBB.

3.4 Problems

Selecting the right cells to be integrated into BBB-on-chip devices is not an easy task as the specific limitations of each cellular model will impact the relevance of findings. Immortalized brain endothelial cell lines have both non-physiological characteristics and weak barrier properties, whereas primary brain endothelial cells are subject to species differences or are hard to source (Fig. 4). Future generations

Table 2 Brain endothelial cells used in BBB-on-chip models[2–6,21–30,32,33,35,37,40,46–67]

Brain endothelial cell lines

Species	Specification	Co-culture	TEER ($\Omega \times cm^2$)	Tracer molecule	Permeability ($P_{app} \times 10^{-6}$ cm s^{-1})	Ref.
Mouse	bEnd.3	Astrocyte (mouse C8D1A cell line)	150–250	FITC–dextran 4 kDa	3.0–5.0	2
				FITC–dextran 20 kDa	2.0	
				FITC–dextran 70 kDa	0.85	
		—	170–230	FITC–dextran 4 kDa	4.0–7.0	25
		Glioma (rat C6 cell line)	220–290	ND	ND	46
		Astrocyte (mouse C8D1A cell line)	ND	FITC–dextran 70 kDa	Relative unit	26
		—	160–180	FITC–dextran 4 kDa	0.48	47
				FITC–dextran 20 kDa	0.35	
				FITC–dextran 500 kDa	0.09	
	cerebEND	—	ND	ND	ND	48
Rat	RBE4	Astrocyte (rat primary embryonic), neuron (rat primary embryonic), microglia (rat primary embryonic)	ND	Alexa 488-dextran 3 kDa	Relative unit	49
		—	ND	FITC–dextran 3–5 kDa	Relative unit	21
Human	hCMEC/D3	—	120	ND	ND	24
		Glioma (human U251 cell line)	ND	Fluorescein, 376 Da	Relative unit	29
				FITC–dextran 70 kDa	Relative unit	
		—	25–35	Fluorescein, 376 Da	1.57	4
				FITC–dextran 4 kDa	1.32	
				Evans-blue albumin, 67 kDa	0.15	
		—	20–30	ND	ND	28
		Pericyte (human cell line, ND), astrocyte (human fetal hTERT cell line), glioblastoma (human U87 cell line)	ND	Sucrose, 342 Da	4.5	22
				FITC–dextran 10 kDa	1.4–6.8	
		Astrocyte (human NHA cell line)	ND	FITC–dextran 4 kDa	1.51	50
		Astrocyte (primary HA, passage number ND), glioma (human U87 cell line)	56–75	Alexa 647-dextran 10 kDa	Relative unit	51
Human	hCMEC/D3	Pericyte (primary HBVP, passage 2–10), astrocyte (human, differentiated from neural stem cells), neuron (human, differentiated from neural stem cells)	ND	FITC–dextran 4 kDa	Relative unit	52
				FITC–dextran 70 kDa	0.3–1.4	
		—	ND	Lucifer yellow, 457 Da	P_e: 26.8	53
				FITC–dextran 10 kDa	P_e: 15.2	
		Pericyte (primary HBVP, passage number ND), astrocyte (primary HA, passage number ND)	5400–12 480	Fluorescein, 376 Da	4.76	54
				FITC–dextran 70 kDa	1.11	
	TY10	Pericyte (human hBPCT cell line), astrocyte (human hAst cell line)	ND	FITC–dextran 20 kDa	Relative unit	35
	HBMEC-IM	Pericyte (primary HBVP, passage 3–5), astrocyte (primary HA, passage 3–5)	130–150	FITC–dextran 4 kDa	1.00	32
				FITC–dextran 40 kDa	0.90	

Primary brain endothelial cells

Species	Name/specification	Co-culture	TEER ($\Omega \times cm^2$)	Tracer molecule	Permeability ($P_{app} \times 10^{-6}$ cm s^{-1})	Ref.
Mouse	MBEC (passage number ND)	—	ND	ND	ND	33
Rat	RBEC (passage 1)	Pericyte (rat primary, passage 1), glial cells (rat primary, passage 1)	114–140	Fluorescein, 376 Da	1.15	4
				FITC–dextran 4 kDa	0.20	
				Evans-blue albumin, 67 kDa	0.04	
Human	HBMVEC (passage 3–8)	Pericyte (primary HBVP, passage 3–8), astrocyte (primary HA, passage 3–8)	ND	Alexa 488-dextran 3 kDa	2.0–4.5	3
	HBMVEC (passage number ND)	Pericyte (primary HBVP, passage number ND), astrocyte (primary HA, passage number ND)	100 Ω (raw data not normalized to surface area)	FITC–dextran 10 kDa	Relative unit	27
	HBMVEC (passage ≤6)	Pericyte (primary HBVP, passage ≤6), astrocyte (primary HA, passage ≤6), neuron (human, differentiated from HIP-009 stem cells)	Relative unit	Cascade blue, 530 Da	11.20	6
				Alexa 555-albumin, 67	0.27	

Table 2 (continued)

Primary brain endothelial cells

Species	Name/specification	Co-culture	TEER ($\Omega \times cm^2$)	Tracer molecule	Permeability ($P_{app} \times 10^{-6}$ cm s^{-1})	Ref.
	HBMVEC (passage 4–10)	Astrocyte (human, differentiated from CDI01434 stem cells), neuron (human, differentiated from Ax0018 stem cells)	7–12	kDa Fluorescein, 376 Da	3.10	23
Human	HBMVEC (passage number ND)	Pericyte (primary HBVP, passage number ND), astrocyte (primary HA, passage number ND), neuron (human, differentiated from neural stem cells), microglia (human HMC3 cell line)	370–400	FITC–dextran 4 kDa	0.58	55
				FITC–dextran 70 kDa	0.08	
	HBMVEC (passage ≤7)	Pericyte (primary HBVP, passage ≤7), astrocyte (primary HA, passage ≤7)	ND	FITC–dextran 10 kDa	0.17	37
				FITC–dextran 40 kDa	0.04	
				FITC–dextran 150 kDa	0.03	

Stem cell-derived brain-like endothelial cells

Species	Name/specification	Co-culture	TEER ($\Omega \times cm^2$)	Tracer molecule	Permeability ($P_{app} \times 10^{-6}$ cm s^{-1})	Ref.
Human	BLEC derived from CD34$^+$ hematopoietic stem cells (umbilical cord blood)	Pericyte-conditioned medium (bovine cell line)	ND	Lucifer yellow, 457 Da	P_e: 8.67	30
		Pericyte (bovine cell line)	250–600	Lucifer yellow, 457 Da	1.40	56
				Evans blue-albumin, 67 kDa	0.14	
		Pericyte (bovine cell line)	ND	ND	ND	40
	iBMEC-derived from iPSCs (line ND)	Pericyte (primary HBVP, passage 3–5), astrocyte (primary HA, passage 3–5)	ND	FITC–dextran 10 kDa	0.2–0.4	5
				FITC–dextran 40 kDa	0.1–0.2	
		Pericyte (primary HBVP, passage 3–5), astrocyte (primary HA, passage 3–5)	ND	FITC–dextran 10 kDa	0.21	57
				FITC–dextran 40 kDa	0.09	
				FITC–dextran 70 kDa	0.06	
	iBMEC derived from iPSCs (CS03iCTR, CS83iCTR, CS0617iCTR, CS0172iCTR, CS0188iCTR lines)	Pericyte (primary HBVP, passage 3), astrocyte (primary HA, passage 3), neuronal progenitors (derived from the same iPSCs)	1000–1500	FITC–dextran 3 kDa	0.09	58
				FITC–dextran 20 kDa	0.1	
	iBMEC-derived from iPSCs (CDIi004-A line)	Pericyte (primary HBVP, passage 3–5), astrocyte (primary HA, passage 3–5), glioblastoma (human GBM22 spheroids)	ND	FITC–dextran 40 kDa	0.03	59
Human	iBMEC-derived from iPSCs (BC1 line)	—	ND	ND	ND	60
		—	ND	FITC–dextran 70 kDa	Relative unit	61
				FITC–dextran 500 kDa	Relative unit	
	iBMEC-derived from iPSCs (IMR90-4 line)	Astrocyte (rat primary, passage 2)	3000–4000	FITC–dextran 4 kDa	0.09	62
				FITC–dextran 20 kDa	0.02	
				FITC–dextran 70 kDa	0.01	
		Pericyte (primary HBVP,	10 000–25 000 Ω	FITC–dextran 3	0.1	63

Table 2 *(continued)*

Stem cell-derived brain-like endothelial cells

Species	Name/specification	Co-culture	TEER ($\Omega \times cm^2$)	Tracer molecule	Permeability ($P_{app} \times 10^{-6}$ cm s^{-1})	Ref.
		passage 3–6), astrocyte (primary HA, passage 3–6)	(raw data not normalized to surface area)	kDa		
				FITC–dextran 10 kDa	0.02	
				FITC–dextran 70 kDa	0.001	
		Pericyte (human primary ACBRI 498, passage number ND), astrocyte (primary HA, passage 2–3)	ND	[13][C]mannitol, 188 Da	0.68	64
				[13][C]sucrose, 342 Da	0.49	
		Astrocyte (primary HA, passage 4)	ND	Lucifer yellow, 457 Da	0.60	65
		—	ND	Lucifer yellow, 457 Da	0.19	66
		Pericyte-conditioned medium (human primary HBVP, passage 3)	750–890	Fluorescein, 376 Da	Relative unit	67
				Alexa 647-dextran 10 kDa	Relative unit	
	EECM-BMEC-like cell derived from iPSCs (IMR90-4 line)	—	ND	Lucifer yellow, 457 Da	P_e: 10.0	53

Abbreviations: BLEC, brain-like endothelial cells; EECM-BMEC, extended endothelial cell culture method brain microvascular endothelial cell; FITC, fluorescein isothiocyanate; HA, human astrocytes; HBMVEC, human brain microvascular endothelial cell; HBVP, human brain vascular pericyte; iBMEC, iPSC-derived brain microvascular endothelial cell; iPSC, induced pluripotent stem cell; MBEC, mouse brain endothelial cell; ND, not determined; P_{app}, apparent permeability coefficient; P_e, endothelial permeability coefficient; RBEC, rat brain endothelial cell.

of BBB-on-chip devices will undoubtedly show a preference for human stem cell-derived brain-like endothelial cells as these offer good scalability and point towards personalized medicine applications. However, the field is divided: brain-like endothelial cells generated using one set of protocols suffer from a non-physiological, mixed epithelial-endothelial identity, whereas others possess a definitive vascular character but have weak barrier properties. In either case, the usability of these models is limited. Added to this, the lack of guidelines on reporting barrier properties in BBB-on-chip devices makes it hard to compare and benchmark results from different laboratories. Quantification of the complex BBB phenotype with different aspects of barrier function is often reduced to a single output given as relative units. While this allows comparisons to be made within a study, such reporting practices serve against the progression of the BBB-on-chip field. A further problem is that few BBB-on-chip models characterize additional BBB properties, like influx- and efflux transporter activity, receptor or adsorptive mediated transcytosis, metabolic activity or glycocalyx integrity.

3.5 Perspectives and recommendations

After a decade of research, the field is getting more conscious about the limitations and challenges of state-of-the art human BBB models. Either the mixed epithelial-endothelial identity or weak barrier characteristics of stem cell-derived models is a rate-limiting step for any future investigation. Therefore, it will be crucial to address these issues in the coming years. We consider it a top priority that novel approaches are developed to enhance BBB properties of human models while still preserving their vascular endothelial character. Promising examples include transcriptional reprogramming using viral vectors[88,91] or targeting a single-[84,92–95] or multiple signaling pathways[15,16] using small molecules. Easy-to-use and affordable approaches that can be readily accessed and used by the whole community are especially favorable.[16]

In addition, future guidelines and improved reporting practices will allow for better comparison and benchmarking of human BBB-on-chip models. We recommend reporting permeability values of BBB models for both small (*e.g.* fluorescein, Lucifer yellow) and large molecular weight tracers (*e.g.* albumin) as this will allow a reliable assessment of both paracellular and transcellular BBB integrity. For instance, a single large molecular weight paracellular tracer (*e.g.* 20, 40 or 70 kDa FITC–dextran) will not predict if the barrier is tight enough for small molecular drug penetration assays. In Table 3, we provide a list of 40 drugs used clinically, endogenous compounds and marker molecules recommended for permeability testing to benchmark BBB-on-chip models. Such experiments should include hydrophilic and lipophilic molecules with passive penetration across the BBB, and compounds with efflux or influx transport mechanisms.[12,16,68,96,97] It is also encouraged that authors report permeability data in commonly accepted international formats, such as apparent (P_{app}) or endothelial (P_e) permeability coefficients,[17,18] instead of relative units. Furthermore, we strongly advise against claims of reaching

Table 3 Examples of drugs, endogenous compounds and markers recommended for permeability testing to benchmark BBB-on-chip models.[12,16,68,96,97] Compounds with human *in vivo* brain penetration data available are highlighted in bold

Transport mechanism	Drug/permeability marker molecule	Endogenous ligand
Passive diffusion, hydrophilic	Atenolol, dextrans (4–70 kDa), fluorescein, inulin, Lucifer yellow, sucrose	Albumin, urea
Passive diffusion, lipophilic	**Antipyrin**, caffeine, **carbamazepine**, **cefotaxime**, diazepam, indomethacin, lamotrigine, **phenytoin**, propranolol, **rolipram**, **trazodone**	ND
Efflux transport	Cimetidine, digoxin, **erlotinib**, loperamide, methotrexate, quinidine, **verapamil**, vinblastine, vincristine	L-Aspartate, L-glutamate
Influx transport	Baclofen, donepezil, **gabapentin**, tacrine, valproic acid	D-Glucose/glucose analogs, L-alanine, L-DOPA, L-arginine, L-lactate

Abbreviations: L-DOPA, L-3,4-dihydroxyphenylalanine; ND, no data on blood–brain barrier models.

'physiological TEER' in human BBB-on-chip models as direct TEER measurements *in vivo* have so far been performed on pial (brain surface) arterial and venous microvessels in anesthetized frogs and rats but not in brain parenchymal capillaries and not in humans.[39] Added to this, the measurement of TEER is influenced by various (generally unreported) factors, such as electrode type and positioning, temperature and viscosity,[39] which is the reason why TEER values can differ by orders of magnitude using the same BBB model reported in different studies (Table 2). Finally, we highlight BBB properties other than paracellular tightness as important aspects to consider and characterize when using BBB-on-chip models. These include but are not limited to 1) confirmation of endothelial properties and morphology, 2) influx- and 3) efflux transporter activity, 4) immune cell adhesion molecule profile and 5) glycocalyx integrity of the BBB-on-chip model.

4. LOC devices to study BBB physiology

4.1 Interactions between neurovascular cell types in BBB-on-chip devices

BBB properties are not intrinsic to brain endothelial cells *in vivo*; rather, they are actively promoted and maintained by organ-specific signaling factors. Barrier properties of cerebral endothelial cells respond to cues from cells of the neurovascular unit and the microenvironment.[1] It has been known for a long time that astrocytes[9] and/or brain pericytes[11,12] induce tighter barrier and other BBB properties in brain endothelial cells when kept in co-culture (Fig. 1). There are several reviews focusing on this topic.[17,18] Most BBB-on-chip models also utilize co-cultures of brain endothelial cells with one or more cell types, including pericytes, astrocytes, neurons (Table 2). Co-culture BBB models from a single species, or even a single source (syngeneic) are ideal for many applications, especially for investigating the effect of a particular genotype on BBB properties. However, we believe that co-culture BBB models from distinct species[30,40,56] are useful tools and express better BBB phenotype than endothelial monocultures. Compared to astrocytes, microglial cells are less applied in

BBB models. Some models use primary glial cultures that contain microglia cells, too,[4] while in other co-cultures microglia cells are specifically added besides astrocytes.[49,55] Despite the widespread use of co-cultures in BBB chips there are few studies which compares them with mono-culture models. The hydrogel based self-organized brain microvascular models are the newest types of BBB-on-chip systems.[5,37] These allow the co-culture of many cell types with direct contact between them recapitulating the *in vivo* anatomical structure. Integration of these chips with biosensors will gather vital physiological parameters and deepen our knowledge on interactions between neurovascular cell types in the future.

Here we would like to mention some examples for the innovative use of chip systems to investigate the physiological role of the BBB and physiological factors that improve BBB properties. In a complex model of the neurovascular system, two BBB chips were connected on each side of a brain chip allowing influx across the BBB, free diffusion with the brain parenchymal compartment and efflux across the BBB.[6] Due to the interaction between the cells of the BBB (brain endothelial cells, astrocytes and pericytes) and the brain compartment (neurons and astrocytes), the neuronal synthesis and secretion of important neurotransmitters, including glutamate and γ-aminobutyric acid (GABA) were significantly increased. This suggests direct neuronal utilization of vascular metabolites and provides evidence that the BBB may play a metabolic role in brain homeostasis. Park *et al.* described a developmentally-inspired induction protocol that includes a 9-day differentiation under hypoxic conditions.[63] In this BBB-on-chip model barrier properties were elevated and maintained over time, the expression of ATP-binding casette (ABC) and solute carrier (SLC) transporters were increased and the functionality of efflux pumps was also improved. The effect of astrocytes or pericytes on brain endothelial cytokine production was investigated on a BBB chip containing a prefabricated microvessel lined with human brain endothelial cells.[3] When stimulated with pro-inflammatory cytokine tumor necrosis factor-α, the secretion of interleukin-6 cytokine was significantly elevated in the chip model in the presence of astrocytes or pericytes. Finally, a microfluidic chip with

transparent nanoporous silicon nitride membrane was developed for live and high-quality imaging of human immune cell interactions with the BBB under physiological flow.[30] In this 2-compartment model adapted to live microscopy stem cell-derived brain-like endothelial cells were cultured on the top of the porous membrane and pericyte-conditioned medium was added to the abluminal chamber. The BBB model showed low permeability and expressed immune cell adhesion molecules which were upregulated upon pro-inflammatory cytokine treatment. The steps of T-cell transmigration could be well studied in this system.[30]

4.2 The effect of shear stress on BBB properties

The effect of shear stress caused by fluid flow has been well documented in peripheral endothelial cells.[98–100] However, much less is known about how shear stress affects BBB properties, including paracellular tightness and tight junction proteins, vesicular transport, efflux pump function or glycocalyx composition specifically in brain endothelial cells. Indeed, few studies have so far investigated the effect of shear stress in BBB-on-chip devices (Table 4).[2–4,24,25,32,46,47,52,55,56,58,60,64] Examples of fluid flow-derived shear stress generation in BBB-on-chip devices are shown in Fig. 5.[4,24,41,101]

Reports on whether shear stress increases paracellular tightness at the BBB are somewhat conflicting. In one of the first papers describing a BBB-on-chip device, Booth and Kim found that TEER was elevated by more than 10-fold in response to shear stress (dyn cm^{-2} not specified).[2] Later studies from the same group demonstrated a 1.35-fold increase in TEER in response to high shear stress (86 dyn cm^{-2}),[25] as well as a 5.8-fold increase in response to 15 dyn cm^{-2}.[46] Despite this increase in TEER, the authors found a statistically non-significant decrease in the permeability of propidium iodide (668 Da) and 4 kDa dextran. Other studies generated lower shear stress values in BBB-on-chip devices. Yet, even in a lower shear stress range, the effect of fluid flow on BBB integrity seems highly context-dependent, and reported changes in TEER do not universally predict changes in permeability (Table 4). For example, Griep et al.[24] reported a 3-fold increase in TEER by a shear stress of 5.8 dyn cm^{-2}, whereas Lyu et al.[55] have measured a 2.2-fold increase in TEER at 3.4 dyn cm^{-2} that was accompanied by an 82% and 90% decrease in the permeability of 4 kDa and 70 kDa dextrans, respectively. Our group have demonstrated a more modest, 1.2-fold increase in TEER in a stem cell-derived model of the BBB (measured at 0.4 and 1.6 dyn cm^{-2}), which was accompanied by an 80% and 90% decrease in the permeability of Lucifer yellow (457 Da) and Evans blue-albumin (67 kDa), respectively.[56] In a previous work we have shown a 1.47-fold increase in TEER at 0.15 dyn cm^{-2} across monolayers of the human hCMEC/D3 cell line but found no increase in TEER in a rat primary brain endothelial cell–pericyte–astrocyte co-culture model at the same level of shear stress.[4] The permeability of fluorescein (376 Da) and 4 kDa

dextran were not changed in either of these models upon dynamic culture in the same study, however, the permeability of Evans blue-albumin was decreased by 60% in hCMEC/D3 cells and more than 80% across the rat primary BBB model.[4]

We have also found contrasting results in BBB-on-chip studies regarding the expression of tight junction proteins and other BBB properties in response to shear stress. Tight junction proteins zonula occludens 1 (ZO-1) and occludin were upregulated upon fluid flow and had a more continuous staining pattern at cell borders in some studies,[25,52,55,58] but not in others.[56,60,64] In studies where an increase in the expression of ZO-1 and occludin was reported, higher increases were seen at higher shear stress levels.[58] This 'dose-dependent' effect was also seen by Garcia-Polite et al. up until 20 dyn cm^{-2} but not above.[102] Claudin-5, the main tight junction protein at the BBB,[103,104] was also induced by 2–2.5-fold upon fluid flow as reported by Lyu et al.[55] and Garcia-Polite et al.[102] Conversely, other studies demonstrated a downregulation of *Cldn5* mRNA by shear stress[56,58] and a change in the localization of claudin-5 protein from tight junctions to intracellular vesicles.[47] As the subcellular distribution of tight junction proteins is supported by the underlying cytoskeleton, it also has to be noted that a characteristic endothelial response to fluid flow, elongation and alignment of cells in the direction of flow, has been reported in some stem cell-derived BBB models with endothelial identity,[56] but not in models with a mixed epithelial–endothelial identity.[58,60,63,64] Glycocalyx acts as an important element of the protection systems of the BBB and also as a mechanosensor of blood flow,[105] yet it is a neglected area in BBB research. Shear stress increased the expression of genes related to glycocalyx remodelling and the intensity of sialic acid staining on the cell surface, and resulted in a more negative surface charge in human brain-like endothelial cells in a chip device.[56] The effect of shear stress on the expression of efflux pumps was investigated by only a handful of studies (Table 4). Kim et al. reported a 1.2-fold increase (dyn cm^{-2} not specified),[52] and Booth et al.[25] reported a 6-fold increase (86 dyn cm^{-2}) in protein levels of P-glycoprotein upon shear stress, whereas no difference was seen in efflux pump mRNA and protein levels in other studies.[56,58,60,64] Taken together, these results highlight a disparity in the literature regarding the effects of shear stress on BBB properties that has to be addressed in future work.

4.3 Problems

One of the major problems related to shear stress used in BBB-on-chip models is that there are no physical measurements of shear stress on human brain microvessels. The reported range of shear stress values in microvascular networks spans three orders of magnitude from less <1 to > 100 dyn cm^{-2} based on measurements on peripheral blood vessels, computational simulations and network modeling.[106] In addition, shear stress values highly depend on the local geometry of microvessels including curvature, bifurcations

Table 4 The effect of shear stress on BBB properties in chip models[2–4,24,25,32,46,47,52,55,56,58,60,64]

Species	Brain endothelial cell	Co-culture	Shear stress (dyn cm^{-2})	Effect on TEER	Effect on tracer permeability	Effect on other BBB properties	Ref.
Mouse	bEnd.3 cell line	Astrocyte (mouse C8D1A cell line)	ND	↑ (10-fold)	ND	ND	2
Human	hCMEC/D3 cell line	—	5.8	↑ (3-fold)	ND	ND	24
Mouse	bEnd.3 cell line	—	0.35–86	↑ (1.35-fold)	Propidium iodide, 668 Da: no change FITC–dextran 4 kDa: ↓ (trend, statistically not significant)	ZO-1 ↑ (5-fold, WB) P-gp ↑ (6-fold, WB)	25
Mouse	bEnd.3 cell line	Glioma (rat C6 cell line)	15	↑ (5.8-fold)	ND	ND	46
Human	hCMEC/D3 cell line	—	0.15	↑ (1.5-fold)	Fluorescein, 376 Da: no change FITC–dextran 4 kDa: no change Evans blue-albumin, 67 kDa: ↓ (60% decrease)	Endothelial morphology: elongation, alignment in the direction of flow (ICC)	4
Rat	Primary RBEC (passage 1)	Pericyte (rat primary, passage 1), glial cells (rat primary, passage 1)	0.15	No change	Fluorescein, 376 Da: no change FITC–dextran 4 kDa: no change Evans blue-albumin, 67 kDa: ↓ (80% decrease)	Endothelial morphology: elongation, alignment in the direction of flow (ICC)	4
Human	Primary HBMVEC (passage 3–8)	Pericyte (primary HBVP, passage 3–8), astrocyte (primary HA, passage 3–8)	1	ND	ND	Characteristic endothelial inflammatory response ↑ (cytokine release)	3
Human	iBMEC derived from iPSCs (BC1 line)	—	4, 12	ND	ND	Claudin-5: no change (ICC) Occludin: no change (ICC) ZO-1: no change (ICC) Cell morphology: no change (ICC)	60
Mouse	bEnd.3 cell line	—	1, 6	ND	ND	Claudin-5: ↓ and localization changes from plasma membrane to intracellular vesicles (ICC)	47
Human	iBMEC derived from iPSCs (CS03iCTR, CS83iCTR, CS0617iCTR, CS0172iCTR, CS0188iCTR lines)	Pericyte (primary HBVP, passage 3), astrocyte (primary HA, passage 3), neuronal progenitors (derived from the same iPSCs)	0.01, 0.5, 2.4	ND	ND	Claudin-5: ↓ (RNA-seq) Occludin: ↑ (RNA-seq) ZO-1: ↑ (RNA-seq) Cell morphology: no change (ICC)	58
Human	HBMEC-IM cell line	Pericyte (primary HBVP, passage 3–5), astrocyte (primary HA, passage 3–5)	4	↑ (1.38-fold)	ND	ND	32
Human	hCMEC/D3 cell line	Pericyte (primary HBVP, passage 2–10), astrocyte and neuron (human, differentiated from neural stem cells)	6	ND	ND	ZO-1 ↑ (1.2-fold, qRT-PCR) P-gp ↑ (1.2-fold, qRT-PCR)	52
Human	HBMVEC (passage number ND)	Pericyte (primary HBVP, passage number ND), astrocyte (primary HA, passage number ND), neuron (human, differentiated from neural stem cells), microglia (human HMC3 cell line)	3.4	↑ (2.2-fold)	FITC–dextran 4 kDa: ↓ (82% decrease), FITC–dextran 70 kDa: ↓ (90% decrease)	Claudin-5: ↑ (2.6-fold, WB) ZO-1: ↑ (2-fold, WB) Endothelial morphology: elongation, alignment in the direction of flow (ICC)	55

Table 4 (continued)

Species	Brain endothelial cell	Co-culture	Shear stress (dyn cm^{-2})	Effect on TEER	Effect on tracer permeability	Effect on other BBB properties	Ref.
Human	BLEC derived from CD34$^+$ hematopoietic stem cells (umbilical cord blood)	Pericyte (bovine cell line)	0.4, 1.6	↑ (1.2-fold)	Lucifer yellow, 457 Da: ↓ (80% decrease)	Claudin-5: ↓ (MACE-seq) Occludin: no change (MACE-seq) ZO-1: no change (MACE-seq)	56
					Evans blue-albumin, 67 kDa: ↓ (90% decrease)	Endothelial glycocalyx: ↑ (core proteins and enzymes, MACE-seq, WGA lectin staining) Endothelial cell surface charge: more negative (laser Doppler velocimetry) Endothelial morphology: elongation, alignment in the direction of flow (ICC)	
Human	iBMEC derived from iPSCs (IMR90-4 line)	Pericyte (human primary ACBRI 498, passage number ND) astrocyte (primary HA, passage 2–3)	0.15, 1.5, 3	ND	^{13}[C]mannitol, 188 Da: ↓ (30–45% decrease)	ZO-1: no change (ICC)	64
					^{13}[C]sucrose, 342 Da: ↓ (50–70% decrease)	Cell morphology: no change (ICC)	

Abbreviations: BLEC, brain-like endothelial cells; FITC, fluorescein isothiocyanate; HA, human astrocytes; HBMVEC, human brain microvascular endothelial cell; HBVP, human brain vascular pericyte; iBMEC, iPSC-derived brain microvascular endothelial cell; ICC, immunocytochemistry; iPSC, induced pluripotent stem cell; MACE-seq, massive analysis of cDNA ends RNA sequencing; ND, not determined; P_{app}, apparent permeability coefficient; P_e, endothelial permeability coefficient; P-gp, P-glycoprotein; RBEC, rat brain endothelial cell; RNA-seq, RNA sequencing; qRT-PCR, quantitative real-time reverse-transcription polymerase chain reaction; WB, western blot; WGA, wheat germ agglutinin; ZO-1: zonula occludens protein 1.

and anastomoses.[106] This means single shear stress values cannot be considered as representative for the different parts of the cerebral vascular bed making comparisons between *in vivo* and *in vitro* data difficult. As Table 4 shows, shear stress values in BBB-on-chip models vary between 0.15–86 dyn cm^{-2} highlighting the diversity of model systems. In addition, the effect of shear stress depends on both physical parameters, like laminar or disturbed flow, magnitude and duration, as well as on endothelial properties (large *vs.* microvessel origin or organ specificity). Therefore, shear stress can induce opposite effects on endothelial junctions, F-actin structure and permeability.[106] The contradictory results on barrier and other properties shown in Table 4 can be explained not only by the different chip devices and shear stress values, but also the very different BBB cellular models used.

4.4 Perspectives

BBB-on-chip models provide an ideal platform for integrating multiple cell types of the neurovascular unit, creating a local microenvironment with dynamic flow conditions. Therefore, more and more BBB-on-chip models use brain endothelial cells together with pericytes, astrocytes, neurons and microglia. Ideally, these cells come from the same species or even the same tissue/cell source. However, we rather recommend co-culture BBB models from distinct species than the use of endothelial monocultures. This might be in the form of co-cultures separated by membranes or microstructures, or as the field moves towards three-dimensional co-cultures with direct contact between the cells, by the addition of brain organoids containing multiple brain cell types as well as by culturing cells in hydrogel-based chip devices allowing the formation of self-organized brain microvascular networks. It will be essential to integrate biosensors in the chip systems to measure multiple physiological BBB parameters including barrier integrity and secretion of biomolecules, but except for TEER measurement, this area is still in its infancy.[20] We anticipate that complex BBB-on-chip co-culture systems will be key to deepen our understanding of cell–cell interactions at the neurovascular unit in the upcoming years.

There is a need for systematic biophysical studies on how physiological flow components affect BBB properties. These should cover the effects of microchannel/microvessels geometry, shear stress ranges, static pressure (mimicking blood pressure) and fluid viscosity. The field would greatly benefit from guidelines related to shear stress and the
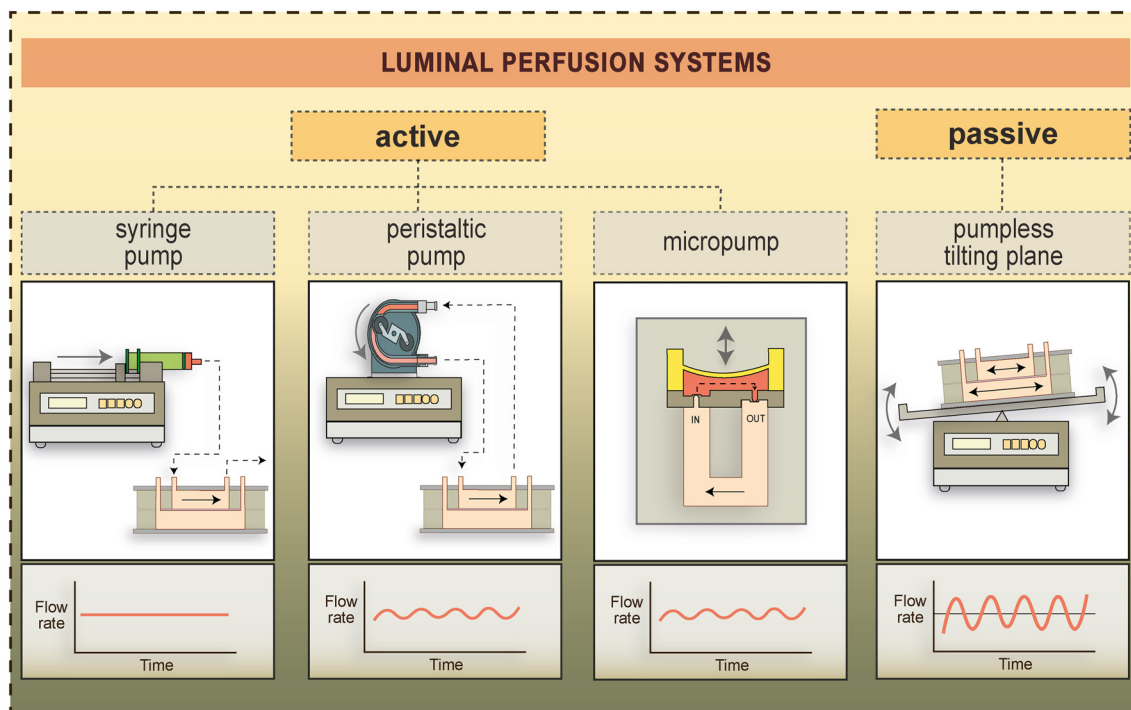
Fig. 5 Types of active and pump-free luminal perfusion systems used to generate fluid flow-induced shear stress in BBB-on-chip devices.[4,24,41,101] Flow rates generated by these methods over time are schematically shown in the lower panels.

measurement of complex BBB properties in different chip models. Other microenvironmental cues, such as brain endothelial plasma membrane curvature due to three-dimensional culture[107] as well as basement membrane composition[108] and stiffness,[109] are getting more recognition as important regulators of BBB function. It is expected that future studies using BBB-on-chip models will shed more light on these aspects under dynamic flow conditions, too. The long-term goal of this area is to integrate BBB-on-chips to human body-on-chip systems that can replace animal models whenever possible. To this end measuring and validating physiological parameters of BBB-on-chips is a key step before microphysiological systems become widely used for disease modelling, drug discovery and personalized medicine.[19]

5. LOC devices to study BBB pharmacology and toxicology

The therapeutic efficacy of neurotherapeutic drugs and nanomedicines depends on their ability to cross the BBB. Therefore, in the last two decades, extensive research efforts have been devoted to the design and validation of new types of cell culture BBB models to better estimate the passage of these therapeutics across the BBB.[110] The fast progress of these models has also been facilitated by the emergence of an unprecedented new law, signed by the FDA in December 2022,[111] which allows full reliance on animal-free alternatives before new drugs are enrolled in human studies.[112] In contrast to other 3D BBB models, such as hydrogel- and spheroid-based models, some of the newly developed

microfluidic-based BBB models allow quantitative permeability measurements and easier comparisons of *in vitro* data with *in vivo* values. Although the number of BBB models in chip devices designed for studying the transport of therapeutic drugs or nanoparticles across the BBB is steadily increasing in the literature, most current models are still far from being a high-throughput screening tool for predicting BBB permeability. In this part of the review only those articles will be discussed in which permeability coefficients were calculated or other well-specified permeability data were given to ensure comparability and usability.

5.1 BBB-on-chip systems for drug penetration measurements

In the last ten years, a wide variety of microfluidic chip-based cell culture platforms (Table 5)[22,29,35,46,62,63,66] were fabricated to investigate the BBB crossing of drugs and drug candidates. Early papers examined the penetration levels of paracellular marker molecules only, which reflect barrier tightness and the applicability of the systems to test the transfer of small drug molecules. In general, fluorescently labelled tracers, mainly dextran, were used in the majority of the studies (Table 5). Booth and Kim[46] demonstrated one of the first permeability studies of different central nervous system drugs in a dynamic microfluidic BBB model and compared the results to *in vivo* data. The penetration of seven drugs, ethosuximide, gabapentin, sertraline, sunitinib, traxoprodil, varenicline, PF-304014, was analyzed in both dynamic and static conditions on bEnd.3 mouse brain endothelial cell line in mono-culture, or in co-culture with C6 rat glial cell line.[46]

Table 5 BBB-on-a-chip systems for molecule and drug penetration[22,29,35,46,62,63,66]

Chip type	Cell types	Drug/molecule	P_{app}/P_e (10^{-6} cm s^{-1})	Analytical methods	Ref.
μBBB chip 2-channel, membrane separated, microfluidic chip	bEnd.3 mouse brain endothelial cell line, C6 rat glial cell line, co-culture	Gabapentin Traxoprodil Sertraline Varenicline Ethosuximide Sunitinib PF-3084014	P_e: 109 ± 7 P_e: 131 ± 37 P_e: 208 ± 20 P_e: 163 ± 78 P_e: 128 ± 10 P_e: 87 ± 13 P_e: 93 ± 12	LC–MS	46
2-channel, membrane separated, microfluidic chip connected to detection chip unit	hCMEC/D3 human brain endothelial cell line, U-251MG human glioma cell line, co-culture	Fluorescein FITC–dextran 70 kDa Sunitinib	P_{app}: 7.16 ± 0.81 P_{app}: 1.41 ± 0.15 P_{app}: 55.7 ± 0.52	ESI-Q-TOFMS	29
BBBoC 2-channel, membrane separated, microfluidic chip	IMR90-4 human iPSC cell line-derived brain endothelial cells, rat primary astrocytes, co-culture	FITC–dextran 4 kDa FITC–dextran 20 kDa FITC–dextran 70 kDa Caffeine Cimetidine Doxorubicin	P_{app}: 0.2 P_{app}: 0.07 P_{app}: 0.02 P_{app}: 485 ± 184 P_{app}: 1.11 ± 0.09 P_{app}: 0.154 ± 0.066	Fluorescence spectrophotometry, LC–MS/MS	62
OrganoPlate BBB-on-chip three-lane, 2-channel, hydrogel based, microfluidic	TY10 human brain endothelial cell line, hAst human astrocyte cell line, hBPCT human brain pericyte cell line, co-culture	Mouse mAb IgG1 Mouse mAb anti-hTfR (MEM-189)	P_{app}: 16 P_{app}: 29	Fluorescence microscopy and image analysis; quantitative immunoassay	35
2-channel, membrane separated, microfluidic chip	IMR90-4 human iPSC cell line-derived brain endothelial cells, human primary astrocytes, human primary brain pericytes, co-culture	FITC–dextran 3 kDa FITC–dextran 10 kDa FITC–dextran 70 kDa Doxorubicin	P_{app}: 0.089 P_{app}: 0.011 P_{app}: 0.002 P_{app}: 0.014	Fluorescence spectrophotometry, MS	63
μBBB chip 3-channel, microchannel-scaffold-separated, microfluidic chip	hCMEC/D3 human brain endothelial cell line, human astrocyte cell line, human pericyte cell line, and U-87 human glioblastoma cell line, co-culture	FITC–dextran 10 kDa Sucrose Nitrofurantoin Caffeine Glucose Alanine	P_{app}: 1.4 P_{app}: 4.5 P_{app}: 3.8 P_{app}: 26.4 P_{app}: 14.9 P_{app}: 18.8	HPLC, fluorescence spectroscopy, beta scintillation counting	22
OrganoPlate BBB-on-chip three-lane, 2-channel, hydrogel based, microfluidic	IMR90-4 human iPSC cell line-derived brain endothelial cells, mono-culture	Lucifer yellow Antipyrine L-Arginine L-Glutamate L-Lactate Quinidine Gabapentin Atenolol Dantrolene	P_{app}: 0.19 P_{app} A–B: 33.4/B–A: 35.1 P_{app} A–B: 14.1/B–A: 5.77 P_{app} A–B: 6.21/B–A: 6.10 P_{app} A–B: 34.1/B–A: 8.74 P_{app} A–B: 21.6/B–A: 22.8 P_{app} A–B: 16.0/B–A: 6.40 P_{app} A–B: 0.8/B–A: 0.6 P_{app} A–B:	Fluorescence spectrophotometry, LC–MS/MS	66

Table 5 *(continued)*

Chip type	Cell types	Drug/molecule	P_{app}/P_e $(10^{-6}$ cm s^{-1})	Analytical methods	Ref.
		Cladribine	14.1/B–A: 50.9 P_{app} A–B: 2.69/B–A: 15.1		

Abbreviations: A–B, apical to basal direction; B–A, basal to apical direction; BBB, blood–brain barrier; BBBoC, blood–brain barrier-on-a-chip system; ESI-Q-TOFMS, electrospray ionization-quadrupole-time of flight-mass spectrometry; LC–MS/MS, liquid chromatography with tandem mass spectrometry; FITC, fluorescein isothiocyanate; HPLC, high performance liquid chromatography; iPSC, induced pluripotent stem cells; LC–MS, liquid chromatography–mass spectrometry; mAb monoclonal antibody; µBBB, microfluidic-based human blood–brain barrier platform; MS, mass spectrometry; P, permeability coefficient; P_{app}, apparent permeability coefficient; P_e, endothelial permeability coefficient.

Drug concentrations were determined by liquid chromatography mass spectrometry (LC–MS). The co-culture BBB model in dynamic condition resulted in significantly higher TEER values and lower drug penetration for all seven drugs compared to mono-culture in chip device or BBB models on culture inserts in static condition. Moreover, the resulting correlation between endothelial permeability coefficients (log P_e) and *in vivo* brain/plasma ratios showed good linear correlation for all model conditions, suggesting the applicability of this microfluidic model for predicting the BBB permeability of centrally acting drugs.[46] Another microfluidic chip device designed specifically for testing neurotherapeutics has the advantage that the penetrated amount of drug was directly measured by an electrospray ionization quadrupole time-of-flight mass spectrometer coupled to the chip.[29] In this 2-channel chip separated by a membrane as a BBB model hCMEC/D3 human brain endothelial cell line was used in mono-culture under fluid flow. The apparent permeability coefficient (P_{app}) value of sunitinib was in the same range as the P_e value of the same compound obtained by the BBB chip designed by Booth and Kim.[46] The higher P_e can be explained by the fact that this type of calculation results in higher values for lipophilic molecules as compared to P_{app}.[96] The chip also contained a separate compartment in which the cytotoxicity of sunitinib that crossed the brain endothelial layer was measured on U-251 human glioma cells cultured in agarose gel. This integrated device allows a rapid analysis of drug candidates by the combination of BBB permeability and cytotoxicity assays as well as drug concentration measurement.[29] A pumpless microfluidic BBB platform was designed by Wang *et al.* using gravity driven flow to reduce wall shear stress.[62] As a BBB model brain endothelial cells were differentiated from IMR90-4 human iPSCs and co-cultured with primary rat astrocytes on the two sides of a porous membrane. These iPSC-differentiated cells had a cobblestone morphology and high TEER values (>3000 Ω cm^2). The model was tested for fluorescently labelled dextrans, large hydrophilic paracellular marker molecules, and model drugs caffeine, cimetidine, and doxorubicin (Table 5). The P_{app} value for caffeine was an order of magnitude higher than in a range of BBB models,[96] while for cimetidine and doxorubicin it was comparable to

literature data.[62] Among the commercially available BBB on chip platforms the two-channel, hydrogel based, microfluidic device OrganoPlate was tested for drug permeability.[35] TY10 human brain endothelial cells were grown in one channel, while human astrocytes and pericytes were grown in a separate channel. Cells in the two channels could communicate through a hydrogel but did not have a direct contact. The barrier functionality was tested by dextran permeability, but the exact value of the permeability coefficient was not indicated in the paper.[35] The penetration of MEM-189 mouse monoclonal antibody specific for human transferrin receptor across the BBB model was 2-fold higher as compared to a control mouse monoclonal IgG1 antibody (Table 5). The concentration of the antibodies was determined by quantitative immunoassay in samples collected from the acceptor compartments of the microdevice.[35] In another study focusing on BBB efflux transporters, the anti-cancer drug, doxorubicin was tested in a human BBB chip where barrier function was induced by hypoxia and flow.[63] The IMR90-4 human iPSC-derived brain endothelial cells were co-cultured with primary human astrocytes and pericytes in a dual-channel, membrane separated chip. This model was the tightest for dextrans based on the P_{app} values (Table 5). Verapamil, a P-glycoprotein inhibitor increased the penetration of doxorubicin ~2.7-fold under flow condition, but blockers of MRP1 or BCRP efflux pumps did not change it, similarly to *in vivo* data. These results indicate high substrate specificity and efflux transporter functionality in this chip model.[63] In a microfluidic chip model integrating BBB and glioblastoma models drugs including caffeine, nitrofurantoin, markers dextran and sucrose, and nutrients glucose and alanine were tested.[22] This system is composed of three channels, a blood and a brain compartment and a medium channel, interconnected by an array of microchannels. In the blood channel hCMEC/D3 brain endothelial cells were co-cultured with astrocytes and pericytes under flow condition. U-87 human glioblastoma cells were seeded in the brain channel. The P_{app} values for paracellular markers dextran and sucrose as well as for the efflux pump ligand nitrofurantoin were low, while the permeability of amphiphilic caffeine and influx transporter ligands glucose and alanine were higher in

agreement with literature data indicating the potential usefulness of this model in drug screening.[22] The most recent chip study measured the permeability for a set of 10 molecules: drugs antipyrine, quinidine, gabapentin, atenolol, dantrolene, cladribine, and amino acids L-arginine, L-glutamate, and L-lactate on the commercially available OrganoPlate platform.[66] As a BBB model IMR90-4 human iPSC cell line-derived brain endothelial cells were used in mono-culture that showed cobble-stone morphology. The low P_{app} of Lucifer yellow indicated a restricted paracellular transport, thus, it was optimal for bidirectional permeability measurement of drugs and endogenous ligands of nutrient transporters (Table 5). The permeability for lipophilic reference molecule antipyrine was high, and it was low for the hydrophilic atenolol.[66] A vectorial transport in the blood to brain (apical to basal) direction was measured for solute carrier ligands L-arginine, L-lactate and gabapentin. Efflux transport in the brain to blood (basal to apical) direction was seen for dantrolene and cladribine.[66] The permeability results for quinidine and L-glutamate, two molecules having efflux transport at the BBB *in vivo*, showed similar P_{app} values in both directions in this model. Brain endothelial cells express solute carriers SLC1A1-3 that actively pump out excitatory amino acids, including the neurotransmitter L-glutamate, at the BBB,[68,113–115] therefore a higher permeability in B–A direction is expected. Quinidine is a ligand of P-glycoprotein resulting also in a permeability directional ratio (PDR) value ≥2 on a primary cell based BBB co-culture model.[97] These data suggest that although this model can predict the permeability of different classes of molecules, it still cannot fully recapitulate BBB properties.

5.2 BBB-on-chip systems for nanoparticle penetration

The number of articles that describe the transfer of nanoparticles in BBB-on-chip systems is constantly increasing. Ideally, non-targeted and functionalized nanocarriers are compared in the same setting (Table 6).[22,32,40,47,50,51,54,57,59,63]

The most investigated targeting ligand for nanoparticles in BBB-on-chip systems was the angiopep-2 peptide targeting low density lipoprotein receptor-related proteins (LRPs) abundantly expressed at the BBB both *in vivo*[113–115] and in culture models.[14,56,87] The penetration of liposomes functionalized with angiopep-2 peptide, was demonstrated across bEnd.3 mouse brain endothelial cell monolayers cultured in the upper compartment of a 2-channel microfluidic device.[47] The permeability of the peptide-targeted liposomes across the BBB model was higher when shear stress induced by fluid flow was induced and also elevated compared to the non-targeted group.[47] Angiopep-2 peptide as a targeting ligand also increased the transfer of quantum dot nanoparticles as compared to a scrambled peptide targeting across an iPSC-derived human brain endothelial cell co-culture model in a chip device.[63] The barrier properties of this model were induced by hypoxia

during the differentiation culture period which was reflected in the very low paracellular permeability of this model (Table 6). Angiopep-2 functionalization was employed for cisplatin loaded nanoparticles to measure their BBB penetration and cancer cell-targeting ability using a self-organized brain microvascular network model and glioblastoma cells in a chip device.[59] The hydrogel based iPSC-derived human brain endothelial cells in the presence of pericytes, astrocytes and glioblastoma cells mimicked the brain tumor vasculature and is a model to study the transition of BBB to blood–tumor barrier. While the penetration of non-targeted and targeted nanocarriers through the BBB model was not different, an improved efficacy of targeted cisplatin loaded polymeric nanoparticles on killing glioblastoma cells was demonstrated both *in vitro* and *in vivo*.[59] Angiopep-2 also facilitated the permeability of gold nanorods designed for theranostic application.[54] The BBB model was a hydrogel-based self-organized microvascular network in a 2-channel microfluidic chip equipped with TEER measurement system. The permeability properties of this BBB model for fluorescein and dextran markers are well fitting literature data (Table 6).

Apolipoproteins A1 and E also interact with LRPs at the BBB and induce receptor mediated transfer of nanoparticles. BBB penetration of high density lipoprotein (HDL)-mimetic lipid nanoparticles targeted with apolipoprotein A1 was demonstrated *via* receptor-mediated transcytosis on a human co-culture BBB model in a more sophisticated microfluidic chip.[32] The lower chamber of the chip device contained three channels. In the central channel human pericytes and astrocytes were embedded in a hydrogel while the lateral channels were filled with culture medium. This setup allows the use of analytical methods to quantify drug or nanoparticle concentrations because the lateral channels enable easy sampling and a simpler permeability coefficient calculation. In another study, a dual-channel chip device with integrated ultrathin silicon nitride membrane was developed to follow nanoparticle transfer by high-resolution imaging.[50] The penetration and subcellular trafficking of apolipoprotein E-conjugated SiO_2 or carboxylate-modified polystyrene fluorescent nanoparticles were investigated. The BBB model consisted of hCMEC/D3 human brain endothelial cells co-cultured with primary human astrocytes and the low P_{app} values for the dextran marker indicated good barrier function (Table 6). Although the permeability of nanoparticles was low, and P_{app} values were not determined, data suggest that size and apolipoprotein E-targeting are principal parameters for NP translocation across the BBB.[50] Another chip device, also designed to yield high resolution images of the trafficking of nanoparticles, had an observation window created using a laser cutting technique in the membrane separating the two channels of the microfluidic chip.[40] In addition to successful imaging of fluorescently labelled HDL particles, the study also conducted diffusion analysis and single molecule tracking. The results proved that although HDL particles interact with the luminal surface of brain

Table 6 BBB-on-a-chip systems for nanoparticle penetration[22,32,40,47,50,51,54,57,59,63]

Chip type	Cell types	Nanoparticle/marker molecule	$P/P_{app}/P_e$ (10^{-6} cm s^{-1})	Analytical methods	Ref.
2-channel, membrane separated, microfluidic chip	bEnd.3 mouse brain endothelial cell line, mono-culture	FITC–dextran 4 kDa FITC–dextran 20 kDa FITC–dextran 500 kDa Non-targeted liposome Angiopep-2-liposomes	P_{app}: 0.48 P_{app}: 0.35 P_{app}: 0.09 P_{app}: 0.02 ± 0.04 P_{app}: 0.16 ± 0.06	Fluorescence spectrophotometry	47
2-channel, membrane separated, microfluidic chip	IMR90-4 human iPSC cell line-derived brain endothelial cells, human primary astrocytes, human primary brain pericytes, co-culture	FITC–dextran 3 kDa FITC–dextran 10 kDa FITC–dextran 70 kDa Scrambled peptide-Qdots Angiopep-2-Qdots	P_{app}: 0.089 P_{app}: 0.011 P_{app}: 0.002 ND ND	Fluorescence spectrophotometry, MS	63
μBBB chip 3-channel, microscaffold-separated, microfluidic chip	hCMEC/D3 human brain endothelial cell line, human astrocyte cell line, human pericyte cell line, and U87-MG human glioblastoma cell line, co-culture	FITC–dextran 10 kDa Albumin-porous silicon NPs Tf-porous silicon NPs	P_{app}: 1.4 ND (RFU ~18) ND (RFU ~40)	HPLC, fluorescence spectroscopy, beta scintillation counting	22
2-channel, hydrogel-based self-organized microvascular network, microfluidic chip	Human iPSC-derived endothelial and brain endothelial cells, human primary astrocytes, human primary brain pericytes, co-culture in 3D fibrin hydrogel	PS NP 100 nm Tf-PS NP 100 nm PS NP 200 nm PS NP 400 nm PU NP 100 nm Tf-PU NP 100 nm	P_{app}: 0.16 ± 0.01 P_{app}: 0.31 ± 3.26 P_{app}: 0.13 ± 0.09 P_{app}: 0.14 ± 0.72 P_{app}: 0.16 ± 1.16 P_{app}: 0.37 ± 2.72	Fluorescence microscopy and image analysis	57
2-channel, membrane separated, hydrogel in lower channel, microfluidic chip	HBMEC human brain endothelial cell line; human primary astrocytes, human primary brain pericytes, co-culture	FITC–dextran 4 kDa FITC–dextran 40 kDa ApoA1-lipid NP (eHNP-A1)	P_{app}: <1.0 P_{app}: <1.0 ND	Fluorescence spectrophotometry, fluorescence microscopy and image analysis	32
μSiM-BBB 2-channel, membrane separated, microfluidic chip	hCMEC/D3 human brain endothelial cell line, primary human astrocytes, co-culture	FITC–dextran 4 kDa Carboxylate-modified PS NP 40 nm Carboxylate-modified PS NP 100 nm ApoE-conjugated SiO$_2$ NP 100 nm	P_{app}: 1.51 165 translocated NPs/24 h 2 translocated NPs/24 h 108 translocated NPs/24 h	Fluorescence spectrophotometry, live-cell fluorescence microscopy and image analysis	50
Microfluidic chip containing 10 prefabricated porous micro-capillaries	hCMEC/D3 human brain endothelial cell line, primary human astrocytes, magnetically-driven spheroids of U87-MG human glioma cell line, co-culture	A647-dextran 10 kDa Anti-TfR mAb-conjugated nutlin-3A-loaded lipid NP 200 nm	ND ND (functional assay: 70% cell death of glioblastoma)	Fluorescence microscopy and image analysis, HPLC	51
2-channel, membrane separated, microfluidic chip	Stem cell-derived human endothelial cell, bovine brain pericyte cell line, mono- and co-culture	Atto647-HDL particles	D: 3 ± 2 × 10^{-3} μm^2 s^{-1}	3D molecule tracking	40
BBB-GBM model 2-channel, hydrogel-based self-organized microvascular network, microfluidic chip	CDIi004-A human iPSC cell line-derived endothelial cells, human primary astrocytes, human primary brain pericytes, spheroids of GBM22 human glioma cell line, co-culture	FITC–dextran 40 kDa PS NP 100 nm pPLD NP >100 nm Angiopep-2-conjugated cisplatin loaded pPLD NP >100 nm	P: 0.026 P: 0.038 P: 0.030 P: 0.020	Fluorescence microscopy and image analysis, flow cytometry	59
BBBoC 2-channel, hydrogel-based self-organized microvascular network, microfluidic chip	hCMEC/D3 human brain endothelial cell line, human primary astrocytes, human primary brain pericytes, co-culture	Fluorescein FITC–dextran 70 kDa D1 peptide-PEG-gold nanorod Angiopep-2/D1 peptide-PEG-gold nanorod	P: 4.76 P: 1.11 P: 3.02 P: 4.74	Fluorescence microscopy and image analysis	54

Abbreviations: anti-TfR mAb, monoclonal antibody against transferrin receptor; ApoA1. apolipoprotein A1; ApoE. apolipoprotein E; BBB, blood–brain barrier; BBBoC, blood–brain barrier-on-a-chip system; D, diffusion constant; FITC, fluorescein isothiocyanate; GBM, glioblastoma multiforme; HDL, high-density lipoprotein; HPLC, high performance liquid chromatography; iPSC, induced pluripotent stem cells; mAb monoclonal antibody; μBBB, microfluidic-based human blood–brain barrier platform; μSIM-BBB, microfluidic-silicon membrane human blood–brain barrier; MS, mass spectrometry; ND, non-detectable; NP, nanoparticle; P, permeability coefficient; P_{app}, apparent permeability coefficient; PEG, polyethylene glycol; pPLD, propargyl poly-L-aspartic acid; PS, polystyrene; PU, polyurethane; Qdots, quantum dots; RFU, relative fluorescence units; SiO$_2$, silicon dioxide; Tf, transferrin; TNFα, tumor necrosis factor alpha.

endothelial cells they do not pass across the *in vitro* BBB co-culture model.[40]

Transferrin receptors are also highly expressed at the BBB, and transferrin, its peptide sequences or antibodies specific for transferrin receptor are widely used to target nanoparticles to brain. As compared to albumin coating transferrin-functionalized porous silicon nanoparticles better crossed a co-culture BBB model integrated with glioblastoma cells in a three-channel (blood, brain, and medium channels) microfluidic chip.[22] In the blood channel, hDMEC/D3 brain endothelial cells, astrocytes, and pericytes were co-cultured under flow condition and U87-MG human glioblastoma cells were seeded in the brain channel. The model showed a good barrier tightness to markers and a drug permeability profile comparable to literature (Table 5). The penetrated nanoparticles targeted glioma cells cultured in the brain compartment.[22] The effect of functionalization with transferrin and nanoparticle size on the penetration was also evaluated in a hydrogel-based self-organized human brain microvascular network in a chip device.[57] The BBB permeability of fluorescent polystyrene and polyurethane nanoparticles with 100, 200 and 400 nm size was calculated by measuring the changes of the fluorescence intensity on confocal images. The effect of the particle size on the penetration across brain endothelial cell layers was evaluated for polystyrene nanoparticles, and no difference was seen in this size range (Table 6). Transferrin functionalization significantly increased the permeability in both types of nanoparticles. The permeability of the marker molecule dextran did not vary during the experiments, indicating that the barrier integrity was preserved. It is important to note that in this model, although it was integrated in a microfluidic device, nanoparticles were not perfused during the permeability experiment.[57]

An anti-transferrin receptor antibody targeted lipid nanocarrier was investigated in a chip containing ten prefabricated porous micro-capillaries.[51] Human brain endothelial cells were cultured on the inner surface of the porous microcapillaries, human primary astrocytes were seeded on the outer surface of the capillaries, and U87 glioblastoma spheroids were kept in 3D magnetically-driven microcages and positioned on top of the microfluidic chip.[51] To test the penetration of nutlin 3A-loaded lipid nanocarriers functionalized with an anti-transferrin receptor antibody, the nanoparticles were perfused inside the microcapillaries and monitored by time-lapse fluorescent imaging. Image analyses demonstrated that the antibody-targeted nutlin-loaded lipid nanocarriers crossed the BBB in sufficient amount, interacted

with glioblastoma spheroids and induced death in 70% of cells indicating anti-tumor potency (Table 6).

5.3 BBB-on-chip systems for toxicity measurements

Few chip systems were described to study the potential toxic effects of drug candidates, therapeutic agents or well-known toxins on the BBB (Table 7).[6,116,117] To study methamphetamine toxicity on a complex neurovascular system two BBB chips were linked to a brain chip allowing separate measurements on the brain and the two influx and efflux BBB compartments.[6] Upon intravascular administration of methamphetamine, a BBB opening effect was preferentially found on the influx BBB chip, whereas no change was detected in the efflux BBB chip.[6]

Organophosphate-based compounds found in pesticides and nerve agents are highly neurotoxic in humans. The effects of four different model organophosphates were investigated on barrier integrity, acetylcholinesterase inhibition, cell viability and residual agent concentration in a dual-channel hydrogel based microfluidic BBB chip.[116] The system contained brain endothelial cells in the vascular channel under fluid flow and neuroblastoma, microglia, and astroglial cells in the extracellular matrix gel compartment. Organophosphates crossed the brain endothelial layer and rapidly inhibited acetylcholinesterase activity. The *in vitro* toxicity ranking of the molecules correlated with available *in vivo* data demonstrating the potential utility of this BBB-on-chip that can be scaled to high throughput as a cost-effective alternative method to animal testing.[116]

Chimeric antigen receptor (CAR)-T cells represent a novel gene-modified cell-based immunotherapy for tumors, including glioblastoma. The efficacy of systemic CAR-T therapy for brain tumors depends on the crossing the BBB, while some CAR-T therapies targeting peripheral tumors may trigger central nervous system side-effects due to BBB disruption. CAR-F263 T cell extravasation across iPSC derived human brain endothelial cells could be visualized and measured in a 3-channel, microscaffold-separated, microfluidic chip.[117] The immune cells effectively killed U87-MG human glioma cells after transmigration, but they also decreased the barrier integrity of the BBB model. The chip model can help to reveal the mechanisms of CAR-T-induced BBB dysfunction and related brain toxicity.[117]

5.4 Problems and perspectives

Despite promising results in the research field there are still no high throughput and widely applicable LOC devices

Table 7   BBB-on-a-chip for toxicology[6,116,117]

Chip type	Cell types	Barrier integrity	Toxic agent/treatment	Effect on barrier integrity	Ref.
Neurovascular organ-on-chip 3 microfluidic chips connected, 2-channel, membrane separated	BBB chips: human primary brain endothelial cells, human primary brain pericytes; brain chip: human primary astrocytes, HIP-009 human hippocampal neuronal stem cells	Cascade blue P_{app}: 11.2 10^{-6} cm s^{-1} Albumin-A555 P_{app}: 0.27 10^{-6} cm s^{-1}	Methamphetamine, 1.5 mM, 24 h	4-fold increase in P_{app} of markers disruption of cellular junctions (VE-cadherin immunostaining)	6
OrganoPlate BBB-on-chip three-lane, 2-channel, hydrogel based, microfluidic	bEnd.3 mouse brain endothelial cell line, C8-D1A mouse astrocyte cell line, N2a mouse neuroblastoma cell line, BV-2 mouse microglia cell line, co-culture	ND	Organophosphates, 24 h DMMP LC_{50} 150 mM DEMP LC_{50} 300 mM DECP LC_{50} 0.4 mM DCP LC_{50} 40 mM	Concentration dependent loss of cellular viability and decreased AChE activity	116
SynBBB 3-channel, microscaffold-separated, microfluidic chip	AF-iPSC human cell line derived brain endothelial cells, U87-MG human glioma cell line	Fluorescein intensity measurement by microscopy and image analysis	CAR-F263 T cells, 48 h	3-fold increase in fluorescein intensity	117

Abbreviations: AChE, acetylcholine esterase; AF-iPSC, human amniotic fluid derived induced pluripotent stem cell line; BBB, blood–brain barrier; CAR, chimeric antigen receptor; DMMP, dimethyl methylphosphonate; DEMP, diethyl methylphosphate; DECP, diethyl cyanophosphonate; DCP, diethyl chlorophosphate; ND, not determined; P_{app}, apparent permeability coefficient; SynBBB, SynVivo blood–brain barrier-on-chip device; VE-cadherin, vascular endothelial cadherin.

validated with a large and diverse drug set to investigate central nervous system drug candidates or delivery systems. Due to the current designs of BBB-on-chips, many challenges limit their applicability in pharmaceutical studies. Use of single pass flow-through fluidic devices decrease drug exposure to study low clearance drugs. Moreover, small medium/buffer volumes make it difficult to obtain kinetic data, minute amount of cells limit the detection of drug metabolism and leakage or evaporation during long-term drug incubations decrease reproducibility. In addition, the standardization and reproducibility of hand-manufactured PDMS-based devices is not always ensured in research laboratories. Automatized production or rigorous quality control would increase the reliability of the chip devices. The adsorbing property of materials for fabrication of microfluidic devices such as PDMS makes testing of small molecules more difficult, they might have impact especially for measuring the bioavailability or recovery of lipophilic drugs.[118] Solutions to this problem could be the correction of drug test results by time and space curves of PDMS adsorption of specific drugs or the use of non-absorbing coatings on the PDMS surface. Novel materials to replace PDMS such as elastomers, hydrogels, thermoplastic polymers, and inorganic materials offer new options for the development of LOC devices in the future.[119] Another major setback for the use of BBB-on-chip models for testing drug candidates is the low number of reliable and comparable studies with proper drug analytical methods. The lack of quantitative drug concentration measurements and calculation of permeability coefficients makes the comparison of results hard on BBB-on-chip models. This is even more problematic in the case of nanocarriers (Table 6).

Ideally, standardized chip devices with low drug absorption, human brain endothelial cell based co-culture BBB model and laminar, one direction, physiological flow conditions should be used for drug or nanoparticle penetration studies. LOC devices with integrated sensors or attached to analytical units could greatly advance the prediction of brain entry of biomolecules and nanocarriers. New legislation allowing clinical trials without animal testing in the USA[111] makes BBB-on-chip models more valuable and important both as predictive tools and alternatives of animal experiments.

6. LOC devices to study BBB pathology

Diverse complex BBB-on-chip models have been developed to study brain disease mechanisms, such as neurodegenerative diseases, stroke, tumor pathology and more (for reviews see[119–121]). Damage of BBB function can often also lead to neuroinflammation, while systemic inflammation caused by viral, bacterial or fungal infections can lead to brain and microvessel dysfunction.[122,123] Therefore, this part of the review focuses on neuroinfections and neuroinflammation (Table 8),[3,24,27,33,49,52,58,124–133] research areas where BBB-on-chip models are particularly useful to discover the background of neuroinflammation and infection mechanisms at the brain microvessel level.

6.1 Neuroinfections

During SARS-CoV-2 infection not only the lung is affected, but infected people can also present a wide variety of neurological symptoms.[134] Buzhdygan *et al.* investigated the

effects of the SARS-CoV-2 spike protein in a tubular, hydrogel-based microfluidic device.[124] They found that in their human brain endothelial cell line-based model barrier integrity was decreased and intercellular junctional staining was weakened after treatment with the S1 subunit of the spike protein (Table 8). Recently it has been shown, that direct infection with SARS-CoV-2 only slightly affected barrier functions at the BBB level in a human brain endothelial cell–astrocyte–microglia dual-compartment biochip model.[126] But if cultured brain endothelial cells received conditioned medium from a SARS-CoV-2 infected alveolar biochip consisting of human pulmonary alveolar epithelial cells and microvascular endothelial cells, barrier properties declined greatly with the loss of tight junction functions, elevated permeability and cell density decrease. Along with these changes observed at the endothelial level, glial activation, proinflammatory cytokine level increase and a wide range of gene expression alterations were observed related to junctional and actin cytoskeletal remodeling.[126]

To counteract the negative effects of Venezuelan equine encephalitis virus (VEEV) on BBB integrity, the effects of omaveloxolone, a small molecule inhibitor that modulates the ubiquitin proteasome signaling pathway was tested in a human cell-based BBB-on-chip with gravity flow.[125] Omaveloxolone decreased virus titer in the cultures, protected against the barrier damaging effect of VEEV and also inhibited the proinflammatory cytokine production after infection with both live attenuated and virulent VEEV strains.[125]

The most common meningitis causing fungus, *Cryptococcus neoformans* and its interaction with human neurovascular unit cells was investigated using a gravity-driven, hydrogel embedded biochip.[52] It was observed, that fungi traverse the brain endothelial cell layer by transcytosis without disrupting tight junctions or creating holes in the endothelial layer. *C. neoformans* forms clusters on the cultured brain endothelial cells and angiogenesis inducing factors are secreted facilitating transmigration.[52]

6.2 Neuroinflammation

The first models to study the effect of TNFα, a proinflammatory cytokine on cultured brain endothelial cells within a LOC device were constructed ten years ago.[24,49] Here authors first assessed the barrier tightness of the models with basic permeability, resistance and immunofluorescent staining tests for intercellular junctions. Treatment with TNFα was performed to confirm that the models work according to previously described data.[135] Stimulation with TNFα increased barrier permeability of cultured brain endothelial cells, elevated the expression of cell adhesion molecules on brain endothelial cells and activated glial cells.[17] In the first two BBB-on-chip devices exposure of brain endothelial cell lines RBE4 and hCMEC/D3 to TNFα treatment increased the permeability, decreased TEER and

co-cultured neurovascular unit cells showed activated morphology (Table 8). Herland *et al.* also showed that when human brain microvascular endothelial cells are co-cultured with human brain pericytes or astrocytes in a tubular BBB chip model embedded in collagen gel elevated cytokine release can be observed after TNFα stimulation.[3] It was confirmed, that the interaction and the presence of astrocytes or pericytes are needed for a response to the pro-inflammatory stimuli. A difference in cytokine secretion after TNFα addition was found between the static culture insert models and the dynamic tubular chip model. In a more recent tubular biochip system based on immortalized human cells, six different types of neurovascular unit composing cell types were embedded in a hydrogel around the brain endothelial cell compartment.[128] Upon LPS stimulation brain endothelial cells showed a weakened barrier integrity, but only when kept in monoculture. Cell adhesion molecule ICAM-1 expression was upregulated and microglia showed an activated phenotype. Cytokine levels were measured from the conditioned medium derived from the model showing upregulation in cytokine levels promoting cell–cell and cell–matrix connection reorganization and destabilizing the barrier integrity.[128]

BBB response to inflammatory stimuli induced by LPS or a cytokine cocktail was studied in a two-compartment LOC device.[27] The authors not only showed that after the addition of the inducing factor BBB permeability increased and resistance decreased, but also that the barrier integrity and intercellular junctional proteins recover with time after the treatments. The analysis of metabolic pathways was performed with mass spectrometry followed by a pathway mapping.

To measure real-time cytokine secretion that enables cytokine profiling of cultured brain endothelial cells a BBB-on-chip system integrated with an immunosensor, named DigiTACK, was introduced.[33] In this two-compartment vertical biochip 500 ng ml^{-1} LPS was used to mimic inflammation induced by bacterial infection, which caused a decrease in the expression of junctional proteins ZO-1 and claudin-5, and an elevated cytokine release both luminally and abluminally.[33]

Recently biotechnological companies started to produce systems for a higher throughput parallel testing. Up to twelve chips can be connected in the system of the company Emulate, in which the two-compartment vertical chip is separated by a thin PDMS membrane. These models also enable the co-culture of multiple cell types next to the brain endothelial cell compartment. The presence of microglia, astrocytes and other cell types of the neurovascular unit were investigated during pro-inflammatory stimulation with TNFα.[58,130] In this model after fluid flow and the formation of a tight barrier by brain endothelial cells human blood was perfused through the vascular channels without any toxic effect on the cells in the brain compartment.[58]

Two-lane and three-lane chips with hydrogel in multi-well plate format, called OrganoPlates were introduced by

Table 8 BBB-on-chip systems to investigate neuroinflammation and infection[3,24,27,33,49,52,58,124–133]

Chip type	Cell type	Inducing factor/pathological agent	Effects on barrier functions	Other effects observed	Ref.
Infection					
One channel cylindrical hydrogel based microfluidic chip	hCMEC/D3 human brain endothelial cell line	SARS-CoV-2 viral spike protein subunit S1 (10 nM)	4 kDa dextran permeability ↑ ZO-1 continuity ↓	—	124
One channel hydrogel based chip with gravity-flow	hCMEC/D3 human brain endothelial cell line, human brain pericytes, human neural stem cell-derived astrocytes and neurons, co-culture	*Cryptococcus neoformans* fungus	Fungal transcytosis tight junctions: no change	Secretion of angiogenesis-inducing factors ↑	52
Two-channel membrane separated microfluidic chip	Primary HBMVECs, brain pericytes and astrocytes	Venezuelan equine encephalitis virus VEEV-TC83 and VEEV-TrD strains	3 kDa dextran permeability ↑	Proinflammatory cytokine level ↑ virus titer in all cells ↑ omaveloxone protection for all parameters	125
Linked two channel membrane separated microfluidic alveolar and BBB chips	Human pulmonary alveolar epithelial cells (HPAEpiCs) and human pulmonary microvascular endothelial cells (HULEC-5a); HBMVECs, HAs, microglial cells (HMC3), peripheral blood mononuclear cells	Direct SARS-CoV-2 infection//indirect infection by conditioned medium exposure from infected alveolar chip	40 kDa dextran permeability ↑ VE-cadherin ↓//permeability ↑ ZO-1, occludin, claudin-5↓ cell density ↓	Conditioned medium treatment: glial and microglial activation matrix metalloproteinase genes ↑ junctional protein and actin cytoskeleton remodeling	126
Neuroinflammation					
Two channel membrane separated microfluidic chip	RBE4 rat brain endothelial cell line, rat primary astrocyte, neuron microglia co-culture	20 ng ml⁻¹ TNFα	3 kDa dextran permeability ↑	ICAM-1 expression ↑ glial activation	49
Two channel membrane separated microfluidic chip	hCMEC/D3 human brain endothelial cell line	1 ng ml⁻¹ TNFα	TEER ↓	—	24
Two channel membrane separated microfluidic chip	Primary HBMVEC + primary HA and pericytes	100 μg ml⁻¹ LPS IL-1β + TNF-α + MCP1,2 (100 ng ml⁻¹ each)	10 kDa dextran permeability ↑ TEER ↓ levels of claudin-5, ZO-1 ↓	Partial recovery of TEER and permeability after LPS treatment with time	27
One channel cylindrical hydrogel based microfluidic chip	HBMVEC, human brain pericytes and astrocytes, co-culture	50 ng ml⁻¹ TNFα	ND	Release of G-CSF, IL-6 and IL-8 ↑ in the presence of astroglia and pericytes	3
Two-compartment scaffold-separated microfluidic chip	HBMVECs, astrocyte-conditioned medium	10 U ml⁻¹ TNFα	40 kDa dextran permeability ↑ TEER ↓ ZO-1 staining intensity ↓	Neutrophil adhesion ↑ all effects blocked by a protein kinase C-delta peptide inhibitor	127
Two-compartment PDMS membrane separated microfluidic chip	iPSC-derived human brain endothelial-like cells and mixed neural culture, primary HAs and brain pericytes	TNFα or IL-1β or IL-8 10 and 100 ng ml⁻¹	3 kDa dextran permeability ↑ cell coverage ↓ relative ZO-1 expression ↓	Retraction of astrocyte protrusions endfeet-like coverage of the vascular surface ↓	58
One channel cylindrical hydrogel based microfluidic chip	Human cell lines: hCMEC/D3 brain endothelial cells, F3.ngn1 neuronal cells, L1.AST astrocytes, HMO6 microglia cells, F3.olig2 oligodendrocytes, L1.PC pericytes	100 μg ml⁻¹ LPS	40 kDa dextran permeability ↑	ICAM-1 expression ↑ microglia activation	128
Two-compartment membrane separated microfluidic chip with branching hierarchy	hCMEC/D3 human brain endothelial cell line	10 ng ml⁻¹ TNFα + heterogeneous shear stress	10 kDa dextran permeability ↑ VE-cadherin continuity ↓	ICAM-1 ↑ expression of P-gp, VE-cadherin and F-actin proteins ↓	129
Two-channel PDMS membrane separated microfluidic chip	iPSC-derived brain endothelial-like cells (iBMECs), glutamatergic and GABAergic neurons, and primary HAs and	100 ng ml⁻¹ TNFα	3 kDa dextran permeability ↑ ZO-1 continuity ↓	ICAM-1 ↑ GLUT-1 expression ↓ IL-1β, IL-6, IFNγ ↑ in the presence of microglia and astrocytes microglia, astrocyte,	130

Table 8 (continued)

Chip type	Cell type	Inducing factor/pathological agent	Effects on barrier functions	Other effects observed	Ref.
Infection					
Two-compartment membrane separated microfluidic chip	brain pericytes, human microglial cell line Human HBMVECs, brain pericytes and astrocytes	10 ng ml^{-1} IL-1β	70 kDa dextran permeability ↑ TEER ↓ ZO-1 continuity ↓	pericyte activation neuronal injury VCAM-1 ↑ protection by omegaven (ω-3 fatty acid emulsion)	131
Two-lane chips with hydrogel in multi-well format	Primary HBMVECs	TNFα + IL-1β (0.12–10 ng ml^{-1} range for each)	Fluorescein permeability ↑ TEER ↓ VE-cadherin expression and continuity ↓	ICAM-1 and VCAM-1 ↑ monocyte adhesion to the endothelial cell surface ↑	132
Two-compartment membrane separated microfluidic chip integrated with cytokine sensor	Primary MBEC	500 ng ml^{-1} LPS	Claudin-5, ZO-1 continuity ↓	Secretion of MCP1, IL-6, CXCL1 chemokines ↑	33
Three channel microfluidic chip, with hydrogel in the middle channel	hCMEC/D3 human brain endothelial cell line, CTX-TNA2 rat brain astrocytes, HMC-3 human microglial cell line	1 µg ml^{-1} LPS	ND	Astrocytic gliosis and microglia activation and migration ↑ protection by 1 µM dexmedetomidine	133

Abbreviations: CXCL1, chemokine (C–X–C motif) ligand 1; GABA, gamma-aminobutyric acid; GLUT-1, glucose transporter-1; G-CSF, granulocyte colony stimulating factor; HA, human astrocytes; HBMVEC, human brain microvascular endothelial cell; HBVP, human brain vascular pericyte; ICAM-1, intercellular cell adhesion molecule-1; IFNγ, interferon-gamma; IL, interleukin; LPS, lipopolysaccharide; MBEC, mouse brain endothelial cell; MCP1, monocyte chemoattractant protein-1; ND, not determined; P-gp, P-glycoprotein; SARS-CoV-2, severe acute respiratory syndrome coronavirus 2; TEER, transendothelial electrical resistance; TNFα, tumor necrosis factor alpha; VCAM-1, vascular cell adhesion molecule 1, VE-cadherin, vascular endothelial cadherin; ZO-1, zonula occludens protein-1.

Mimetas to study BBB changes. Multiple cell types can be seeded in this pump-less system which uses gravity-based fluid flow (Fig. 5). Resistance and permeability can be measured and fluorescent staining can be performed.[132] While these systems provide parallel testing, their use needs expertise and wide experience in handling and studying brain endothelial cells and other neurovascular cell types.

In addition to the investigation of basic phenomena in neuroinflammatory processes, the protection of the brain endothelial cells against damage caused by inflammation needs to be studied, too. Tang *et al.* found that a protein kinase C-delta inhibitor reversed the barrier integrity decrease and adhesion molecule upregulation caused by TNFα stimulation on cultured brain endothelial cells.[127] A clinically available omega-3 fatty acid emulsion, Omegaven, was also effective to counteract the permeability elevation, TEER decrease and junctional disturbance caused by treatment with pro-inflammatory cytokine IL-1β.[131] Dexmedetomidine, an α2 adrenergic receptor agonist with sedative, analgesic and anti-inflammatory properties was also tested in a BBB-on-chip model treated with LPS (Table 8). LPS activated astroglia and microglia cells, and increased the migration of microglia which were decreased or reversed by dexmedetomidine.[133]

6.3 Problems and perspectives

Several approaches have been merged to expand the possibilities to test neuroinflammation in a biochip. There are three main key factors in general which determine the success of a neuroinflammation BBB-on-chip model: (i) brain cell types used, (ii) mono-culture or co-culture of brain endothelial cells with other cells of the neurovascular unit, and (iii) the morphology of the vascular channel and how other parts of the chip are connected to it. Usually brain microvascular endothelial cell types of human or animal tissue origin are introduced to the systems, which can be immortalized cell lines, primary or stem-cell differentiated cells (Fig. 4). Although research using peripheral endothelial cell types, such as HUVEC[136] or cells not forming a monolayer or not expressing proper intercellular junctional morphology[137,138] might contribute to the understanding of systemic or local neuroinflammation on a vessel level, conclusions drawn using these cellular models regarding the brain and BBB should be treated with caution. The next important parameter of a neuroinflammation model is whether mono-culture of brain endothelial cells or co-culture of brain endothelial cells with the other cells of the neurovascular unit is used. To better mimic the interaction between cells and to investigate glial activation in the brain compartment in several models more than 3 types of cells are

introduced into the chip.[128,130] Brain endothelial cells in mono-culture or in co-culture can react completely differently to the same stimulus because of the factors secreted by their neighboring cell types, such as astrocytes, microglia, pericytes or neurons.[3,128,130] The BBB-on-chip setup usually contains two compartments separated by a porous membrane, or brain endothelial cells are grown in a preformed hydrogel tube (Fig. 2). Other cells of the neurovascular unit are generally seeded to the other compartment in a direct or indirect contact with the brain endothelial cells, or they are directly introduced into the hydrogel. In the vessel compartment the introduction of shear stress is crucial to induce signal transduction pathways connected to mechanosensing to create a more physiological milieu in the BBB-on-chip (for details see Table 4 and related section). A novel model even uses a branched tubular channel setup to characterize the combined effects of different vessel sizes and shear stress.[129] A limitation of this model is that brain endothelial cells can only be kept in mono-culture, creating a less complex model to study the aspects of neuroinflammation. Therefore, both the BBB-on-chip model and the research question have to be carefully selected for each approach. The BBB is not only affected in many neurological diseases, but also in neuropsychiatric conditions, where the dysfunction of the BBB leads to the development of the pathology. BBB-on-chip models are almost completely missing from the field of study of neuropsychiatric disorders, such as depression, autism or schizophrenia. Since BBB regulation is compromised in almost all of these conditions,[139] it would be important to develop more physiological and relevant models to reveal the pathomechanisms and to discover new BBB protective drugs.

7. Conclusions and outlook

In this review, we have identified knowledge gaps and pointed out contradictions in the literature of BBB-on-chip models. Importantly, direct measurements on TEER and shear stress are missing in the human brain vasculature, which makes it hard to compare *in vitro* data with *in vivo* physiological values. Indeed, the field relies on measurements that were performed on animals several decades ago, as well as on computational simulations and modeling.[39,106] We still do not fully understand why shear stress makes barrier properties tighter in some endothelial models but weaker in others as shown in Table 4 and as demonstrated in peripheral endothelial cultures.[106] We hope future studies will address these questions in the form of direct *in vitro*/*in vivo* measurements and comparisons, as well as by shedding light on the organ- and zonation-specific effects of shear stress throughout the vasculature.

We have also highlighted neglected engineering and cell biological aspects of BBB-on-chip models that should come into focus in future works. For example, static pressure perpendicular to the direction of flow, which mimics blood pressure, should be considered and reported in chip devices.

We believe that the lack of static pressure could be one of the reasons behind empirical observations that endothelial cells detach from channels when high flow velocities are used. In addition, future experiments should take into account fluid viscosity and the presence of blood cells in the vessel compartment of BBB-on-chip models. Although the composition and stiffness of the extracellular matrix has been shown to play a role in brain endothelial physiology and pathology, these aspects are seldom considered in the field. Finally, current controversies related to the cellular identity of some stem cell-derived brain-like endothelial cells (iBMECs) could be resolved by an unequivocal characterization of vascular endothelial properties and functions. We recommend that these include verifying the expression of endothelial markers (*e.g.* ESAM, PECAM-1, VE-cadherin), endothelial cytoarchitecture and surface glycocalyx, coagulation factors and inhibitors (*e.g.* von Willebrand factor, plasminogen activator inhibitor-1, tissue or urokinase plasminogen activator), and the production of or reaction to vasoactive agents (*e.g.* nitric oxide, prostaglandins, adrenomedullin), which have so far been neglected in stem cell-derived BBB-on-chip models.

The BBB-on-chip field is highly interdisciplinary that combines expertise from materials science, bioengineering as well as stem cell- and vascular/BBB biology. To move the field forward, there is a need for better integration of these diverse disciplines that can only be achieved by setting clear parameters for characterizing both the chip- and the BBB model parts technically and functionally. We highly recommend the use of standardized metrics, such as Ω cm^2 for TEER, permeability coefficients (10^{-6} cm s^{-1}) for permeability, and dyn cm^{-2} for shear stress to ensure that studies utilizing models with different chip geometry and cell types are comparable. Future guidelines with the participation of leading research groups with diverse expertise in the field will greatly help this cause.

Author contributions

Author Contributions: conceptualization, M. A. D., A. D.; writing – original draft preparation, A. K., S. V., F. R. W., J. P. V., A. E. K., S. V., M. M., A. S., G. P., M. A. D., A. D.; writing – review and editing, M. A. D., G. P., A. D.; visualization, A. S., A. K., A. E. K., G. P., M. A. D.; supervision, M. A. D. and A. D., funding acquisition, M. A. D. and A. D.

Conflicts of interest

There are no conflicts to declare.

Acknowledgements

References

1 M. D. Sweeney, Z. Zhao, A. Montagne, A. R. Nelson and B. V. Zlokovic, Blood-brain barrier: from physiology to disease and back, *Physiol. Rev.*, 2019, **99**, 21–78.

2 R. Booth and H. Kim, Characterization of a microfluidic in vitro model of the blood-brain barrier (μBBB), *Lab Chip*, 2012, **12**, 1784–1792.

3 A. Herland, A. D. van der Meer, E. A. FitzGerald, T. E. Park, J. J. Sleeboom and D. E. Ingber, Distinct contributions of astrocytes and pericytes to neuroinflammation identified in a 3D human blood-brain barrier on a chip, *PLoS One*, 2016, **11**, e0150360.

4 F. R. Walter, S. Valkai, A. Kincses, A. Petneházi, T. Czeller, S. Veszelka, P. Ormos, M. A. Deli and A. Dér, Versatile lab-on-a-chip tool for modeling biological barriers, *Sens. Actuators, B*, 2016, **222**, 1209–1219.

5 M. Campisi, Y. Shin, T. Osaki, C. Hajal, V. Chiono and R. D. Kamm, 3D self-organized microvascular model of the human blood-brain barrier with endothelial cells, pericytes and astrocytes, *Biomaterials*, 2018, **180**, 117–129.

6 B. M. Maoz, A. Herland, E. A. FitzGerald, T. Grevesse, C. Vidoudez, A. R. Pacheco, S. P. Sheehy, T.-E. Park, S. Dauth, R. Mannix, N. Budnik, K. Shores, A. Cho, J. C. Nawroth, D. Segrè, B. Budnik, D. E. Ingber and K. K. Parker, A linked organ-on-chip model of the human neurovascular unit reveals the metabolic coupling of endothelial and neuronal cells, *Nat. Biotechnol.*, 2018, **36**, 865–874.

7 P. Panula, F. Joó and L. Rechardt, Evidence for the presence of viable endothelial cells in cultures derived from dissociated rat brain, *Experientia*, 1978, **34**, 95–97.

8 P. D. Bowman, S. R. Ennis, K. E. Rarey, A. L. Betz and G. W. Goldstein, Brain microvessel endothelial cells in tissue culture: a model for study of blood-brain barrier permeability, *Ann. Neurol.*, 1983, **14**, 396–402.

9 M.-P. Dehouck, S. Méresse, P. Delorme, J. C. Fruchart and R. Cecchelli, An easier, reproducible, and mass-production method to study the blood-brain barrier in vitro, *J. Neurochem.*, 1990, **54**, 1798–1801.

10 P. Kása, M. Pákáski, F. Joó and A. Lajtha, Endothelial cells from human fetal brain microvessels may be cholinoceptive, but do not synthesize acetylcholine, *J. Neurochem.*, 1991, **56**, 2143–2146.

11 S. Nakagawa, M. A. Deli, S. Nakao, M. Honda, K. Hayashi, R. Nakaoke, Y. Kataoka and M. Niwa, Pericytes from brain microvessels strengthen the barrier integrity in primary cultures of rat brain endothelial cells, *Cell. Mol. Neurobiol.*, 2007, **27**, 687–694.

12 S. Nakagawa, M. A. Deli, H. Kawaguchi, T. Shimizudani, T. Shimono, Á. Kittel, K. Tanaka and M. Niwa, A new blood-brain barrier model using primary rat brain endothelial cells, pericytes and astrocytes, *Neurochem. Int.*, 2009, **54**, 253–263.

13 E. S. Lippmann, S. M. Azarin, J. E. Kay, R. A. Nessler, H. K. Wilson, A. Al-Ahmad, S. P. Palecek and E. V. Shusta, Derivation of blood-brain barrier endothelial cells from human pluripotent stem cells, *Nat. Biotechnol.*, 2012, **30**, 783–791.

14 R. Cecchelli, S. Aday, E. Sevin, C. Almeida, M. Culot, L. Dehouck, C. Coisne, B. Engelhardt, M.-P. Dehouck and L. Ferreira, A stable and reproducible human blood-brain barrier model derived from hematopoietic stem cells, *PLoS One*, 2014, **9**, e99733.

15 C. Praça, S. C. Rosa, E. Sevin, R. Cecchelli, M. P. Dehouck and L. S. Ferreira, Derivation of brain capillary-like endothelial cells from human pluripotent stem cell-derived endothelial progenitor cells, *Stem Cell Rep.*, 2019, **13**, 599–611.

16 G. Porkoláb, M. Mészáros, A. Szecskó, J. P. Vigh, F. R. Walter, R. Figueiredo, I. Kálomista, Z. Hoyk, G. Vizsnyiczai, I. Gróf, J.-S. Jan, F. Gosselet, M. K. Pirity, M. Vastag, N. Hudson, M. Campbell, S. Veszelka and M. A. Deli, Synergistic induction of blood-brain barrier properties, BioRxiv, 2023, preprint, DOI: 10.1101/2023.02.09.527899.

17 M. A. Deli, C. S. Ábrahám, Y. Kataoka and M. Niwa, Permeability studies on in vitro blood-brain barrier models: physiology, pathology, and pharmacology, *Cell. Mol. Neurobiol.*, 2005, **25**, 59–127.

18 H. C. Helms, N. J. Abbott, M. Burek, R. Cecchelli, P.-O. Couraud, M. A. Deli, C. Förster, H. J. Galla, I. A. Romero, E. V. Shusta, M. J. Stebbins, E. Vandenhaute, B. Weksler and B. Brodin, In vitro models of the blood-brain barrier: An overview of commonly used brain endothelial cell culture models and guidelines for their use, *J. Cereb. Blood Flow Metab.*, 2016, **36**, 862–890.

19 D. E. Ingber, Human organs-on-chips for disease modelling, drug development and personalized medicine, *Nat. Rev. Genet.*, 2022, **23**, 467–491.

20 A. Kincses, J. P. Vigh, D. Petrovszki, S. Valkai, A. E. Kocsis, F. R. Walter, H.-Y. Lin, J.-S. Jan, M. A. Deli and A. Dér, The use of sensors in blood-brain barrier-on-a-chip devices: Current practice and future directions, *Biosensors*, 2023, **13**, 357.

21 B. Prabhakarpandian, M. C. Shen, J. B. Nichols, I. R. Mills, M. Sidoryk-Wegrzynowicz, M. Aschner and K. Pant, SyM-BBB: a microfluidic Blood Brain Barrier model, *Lab Chip*, 2013, **13**, 1093–1101.

22 B. Peng, Z. Tong, W. Y. Tong, P. J. Pasic, A. Oddo, Y. Dai, M. Luo, J. Frescene, N. G. Welch, C. D. Easton, H. Thissen and N. H. Voelcker, In situ surface modification of microfluidic blood-brain-barriers for improved screening of small

molecules and nanoparticles, *ACS Appl. Mater. Interfaces*, 2020, **12**, 56753–56766.

23 N. R. Wevers, A. L. Nair, T. M. Fowke, M. Pontier, D. G. Kasi, X. M. Spijkers, C. Hallard, G. Rabussier, R. van Vught, P. Vulto, H. E. de Vries and H. L. Lanz, Modeling ischemic stroke in a triculture neurovascular unit on-a-chip, *Fluids Barriers CNS*, 2021, **18**, 59.

24 L. M. Griep, F. Wolbers, B. de Wagenaar, P. M. ter Braak, B. B. Weksler, I. A. Romero, P.-O. Couraud, I. Vermes, A. D. van der Meer and A. van den Berg, BBB on chip: microfluidic platform to mechanically and biochemically modulate blood-brain barrier function, *Biomed. Microdevices*, 2013, **15**, 145–150.

25 R. Booth, S. Noh and H. Kim, A multiple-channel, multiple-assay platform for characterization of full-range shear stress effects on vascular endothelial cells, *Lab Chip*, 2014, **14**, 1880–1890.

26 K. L. Sellgren, B. T. Hawkins and S. Grego, An optically transparent membrane supports shear stress studies in a three-dimensional microfluidic neurovascular unit model, *Biomicrofluidics*, 2015, **9**, 061102.

27 J. A. Brown, S. G. Codreanu, M. Shi, S. D. Sherrod, D. A. Markov, M. D. Neely, C. M. Britt, O. S. Hoilett, R. S. Reiserer, P. C. Samson, L. J. McCawley, D. J. Webb, A. B. Bowman, J. A. McLean and J. P. Wikswo, Metabolic consequences of inflammatory disruption of the blood-brain barrier in an organ-on-chip model of the human neurovascular unit, *J. Neuroinflammation*, 2016, **13**, 306.

28 M. W. van der Helm, M. Odijk, J. P. Frimat, A. D. van der Meer, J. C. T. Eijkel, A. van den Berg and L. I. Segerink, Direct quantification of transendothelial electrical resistance in organs-on-chips, *Biosens. Bioelectron.*, 2016, **85**, 924–929.

29 X. Shao, D. Gao, Y. Chen, F. Jin, G. Hu, Y. Jiang and H. Liu, Development of a blood-brain barrier model in a membrane-based microchip for characterization of drug permeability and cytotoxicity for drug screening, *Anal. Chim. Acta*, 2016, **934**, 186–193.

30 A. Mossu, M. Rosito, T. Khire, H. Li Chung, H. Nishihara, I. Gruber, E. Luke, L. Dehouck, F. Sallusto, F. Gosselet, J. L. McGrath and B. Engelhardt, A silicon nanomembrane platform for the visualization of immune cell trafficking across the human blood-brain barrier under flow, *J. Cereb. Blood Flow Metab.*, 2019, **39**, 395–410.

31 A. Kincses, A. R. Santa-Maria, F. R. Walter, L. Dér, N. Horányi, D. V. Lipka, S. Valkai, M. A. Deli and A. Dér, A chip device to determine surface charge properties of confluent cell monolayers by measuring streaming potential, *Lab Chip*, 2020, **20**, 3792–3805.

32 S. I. Ahn, Y. J. Sei, H. J. Park, J. Kim, Y. Ryu, J. J. Choi, H. J. Sung, T. J. MacDonald, A. I. Levey and Y. Kim, Microengineered human blood-brain barrier platform for understanding nanoparticle transport mechanisms, *Nat. Commun.*, 2020, **11**, 175.

33 S. H. Su, Y. Song, A. Stephens, M. Situ, M. C. McCloskey, J. L. McGrath, A. V. Andjelkovic, B. H. Singer and K. Kurabayashi, A tissue chip with integrated digital immunosensors: In situ brain endothelial barrier cytokine secretion monitoring, *Biosens. Bioelectron.*, 2023, **224**, 115030.

34 P. P. Partyka, G. A. Godsey, J. R. Galie, M. C. Kosciuk, N. K. Acharya, R. G. Nagele and P. A. Galie, Mechanical stress regulates transport in a compliant 3D model of the blood-brain barrier, *Biomaterials*, 2017, **115**, 30–39.

35 N. R. Wevers, D. G. Kasi, T. Gray, K. J. Wilschut, B. Smith, R. van Vught, F. Shimizu, Y. Sano, T. Kanda, G. Marsh, S. J. Trietsch, P. Vulto, H. L. Lanz and B. Obermeier, A perfused human blood-brain barrier on-a-chip for high-throughput assessment of barrier function and antibody transport, *Fluids Barriers CNS*, 2018, **15**, 23.

36 M. A. Winkelman, D. Y. Kim, S. Kakarla, A. Grath, N. Silvia and G. Dai, Interstitial flow enhances the formation, connectivity, and function of 3D brain microvascular networks generated within a microfluidic device, *Lab Chip*, 2021, **22**, 170–192.

37 C. Hajal, G. S. Offeddu, Y. Shin, S. Zhang, O. Morozova, D. Hickman, C. G. Knutson and R. D. Kamm, Engineered human blood-brain barrier microfluidic model for vascular permeability analyses, *Nat. Protoc.*, 2022, **17**, 95–128.

38 J. Wegener, S. Zink, P. Rösen and H. Galla, Use of electrochemical impedance measurements to monitor β-adrenergic stimulation of bovine aortic endothelial cells, *Pfluegers Arch.*, 1999, **437**, 925–934.

39 J. P. Vigh, A. Kincses, B. Ozgür, F. R. Walter, A. R. Santa-Maria, S. Valkai, M. Vastag, W. Neuhaus, B. Brodin, A. Dér and M. A. Deli, Transendothelial electrical resistance measurement across the blood-brain barrier: A critical review of methods, *Micromachines*, 2021, **12**, 685.

40 R. Buchroithner, S. Mayr, F. Hauser, E. Priglinger, H. Stangl, A. R. Santa-Maria, M. A. Deli, A. Dér, T. A. Klar, M. Axmann, D. Sivun, M. Mairhofer and J. Jacak, Dual channel microfluidics for mimicking the blood-brain barrier, *ACS Nano*, 2021, **15**, 2984–2993.

41 W. Wei, F. Cardes, A. Hierlemann and M. M. Modena, 3D in vitro blood-brain-barrier model for investigating barrier insults, *Adv. Sci.*, 2023, **10**, 2205752.

42 J. Kieninger, A. Weltin, H. Flamm and G. A. Urban, Microsensor systems for cell metabolism – from 2D culture to organ-on-chip, *Lab Chip*, 2018, **18**, 1274–1291.

43 R. Vashistha, A. K. Dangi, A. Kumar, D. Chhabra and P. Shukla, Futuristic biosensors for cardiac health care: an artificial intelligence approach, *3 Biotech*, 2018, **8**, 358.

44 F. Inci, Benchmarking a microfluidic-based filtration for isolating biological particles, *Langmuir*, 2022, **38**, 1897–1909.

45 B. Weksler, I. A. Romero and P. O. Couraud, The hCMEC/D3 cell line as a model of the human blood brain barrier, *Fluids Barriers CNS*, 2013, **10**, 16.

46 R. Booth and H. Kim, Permeability analysis of neuroactive drugs through a dynamic microfluidic in vitro blood-brain barrier model, *Ann. Biomed. Eng.*, 2014, **42**, 2379–2391.

47 I. Papademetriou, E. Vedula, J. Charest and T. Porter, Effect of flow on targeting and penetration of angiopep-decorated nanoparticles in a microfluidic model blood-brain barrier, *PLoS One*, 2018, **13**, e0205158.

48 D. Sticker, M. Rothbauer, J. Ehgartner, C. Steininger, O. Liske, R. Liska, W. Neuhaus, T. Mayr, T. Haraldsson, J. P. Kutter and P. Ertl, Oxygen management at the microscale: A functional biochip material with long-lasting and tunable oxygen scavenging properties for cell culture applications, *ACS Appl. Mater. Interfaces*, 2019, **11**, 9730–9739.

49 A. K. Achyuta, A. J. Conway, R. B. Crouse, E. C. Bannister, R. N. Lee, C. P. Katnik, A. A. Behensky, J. Cuevas and S. S. Sundaram, A modular approach to create a neurovascular unit-on-a-chip, *Lab Chip*, 2013, **13**, 542–553.

50 D. Hudecz, T. Khire, H. L. Chung, L. Adumeau, D. Glavin, E. Luke, M. S. Nielsen, K. A. Dawson, J. L. McGrath and Y. Yan, Ultrathin silicon membranes for in situ optical analysis of nanoparticle translocation across a human blood-brain barrier model, *ACS Nano*, 2020, **14**, 1111–1122.

51 O. Tricinci, D. De Pasquale, A. Marino, M. Battaglini, C. Pucci and G. Ciofani, A 3D biohybrid real-scale model of the brain cancer microenvironment for advanced in vitro testing, *Adv. Mater. Technol.*, 2020, **5**, 2000540.

52 J. Kim, K.-T. Lee, J. S. Lee, J. Shin, B. Cui, K. Yang, Y. S. Choi, N. Choi, S. H. Lee, J.-H. Lee, Y.-S. Bahn and S.-W. Cho, Fungal brain infection modelled in a human-neurovascular-unit-on-a-chip with a functional blood-brain barrier, *Nat. Biomed. Eng.*, 2021, **5**, 830–846.

53 M. C. McCloskey, P. Kasap, S. D. Ahmad, S. H. Su, K. Chen, M. Mansouri, N. Ramesh, H. Nishihara, Y. Belyaev, V. V. Abhyankar, S. Begolo, B. H. Singer, K. F. Webb, K. Kurabayashi, J. Flax, R. E. Waugh, B. Engelhardt and J. L. McGrath, The modular μSiM: A mass produced, rapidly assembled, and reconfigurable platform for the study of barrier tissue models in vitro, *Adv. Healthcare Mater.*, 2022, **11**, e2200804.

54 S. Palma-Florez, A. López-Canosa, F. Moralez-Zavala, O. Castaño, M. J. Kogan, J. Samitier, A. Lagunas and M. Mir, BBB-on-a-chip with integrated micro-TEER for permeability evaluation of multi-functionalized gold nanorods against Alzheimer's disease, *J. Nanobiotechnol.*, 2023, **21**, 115.

55 Z. Lyu, J. Park, K. M. Kim, H. J. Jin, H. Wu, J. Rajadas, D. H. Kim, G. K. Steinberg and W. Lee, A neurovascular-unit-on-a-chip for the evaluation of the restorative potential of stem cell therapies for ischaemic stroke, *Nat. Biomed. Eng.*, 2021, **5**, 847–863.

56 A. R. Santa-Maria, F. R. Walter, R. Figueiredo, A. Kincses, J. P. Vigh, M. Heymans, M. Culot, P. Winter, F. Gosselet, A. Dér and M. A. Deli, Flow induces barrier and glycocalyx-related genes and negative surface charge in a lab-on-a-chip human blood-brain barrier model, *J. Cereb. Blood Flow Metab.*, 2021, **41**, 2201–2215.

57 S. W. L. Lee, M. Campisi, T. Osaki, L. Possenti, C. Mattu, G. Adriani, R. D. Kamm and V. Chiono, Modeling nanocarrier transport across a 3D in vitro human blood-brain-barrier microvasculature, *Adv. Healthcare Mater.*, 2020, **9**, e1901486.

58 G. D. Vatine, R. Barrile, M. J. Workman, S. Sances, B. K. Barriga, M. Rahnama, S. Barthakur, M. Kasendra, C. Lucchesi, J. Kerns, N. Wen, W. R. Spivia, Z. Chen, J. Van Eyk and C. N. Svendsen, Human iPSC-derived blood-brain barrier chips enable disease modeling and personalized medicine applications, *Cell Stem Cell*, 2019, **24**, 995–1005.

59 J. P. Straehla, C. Hajal, H. C. Safford, G. S. Offeddu, N. Boehnke, T. G. Dacoba, J. Wyckoff, R. D. Kamm and P. T. Hammond, A predictive microfluidic model of human glioblastoma to assess trafficking of blood-brain barrier-penetrant nanoparticles, *Proc. Natl. Acad. Sci. U. S. A.*, 2022, **119**, e2118697119.

60 J. G. DeStefano, Z. S. Xu, A. J. Williams, N. Yimam and P. C. Searson, Effect of shear stress on iPSC-derived human brain microvascular endothelial cells (dhBMECs), *Fluids Barriers CNS*, 2017, **14**, 20.

61 N. Zhao, Z. Guo, S. Kulkarni, D. Norman, S. Zhang, T. D. Chung, R. F. Nerenberg, R. Linville and P. Searson, Engineering the human blood-brain barrier at the capillary scale using a double-templating technique, *Adv. Funct. Mater.*, 2022, **32**, 2110289.

62 Y. I. Wang, H. E. Abaci and M. I. Shuler, Microfluidic blood-brain barrier model provides in vivo-like barrier properties for drug permeability screening, *Biotechnol. Bioeng.*, 2017, **114**, 184–194.

63 T. E. Park, N. Mustafaoglu, A. Herland, R. Hasselkus, R. Mannix, E. A. FitzGerald, R. Prantil-Baun, A. Watters, O. Henry, M. Benz, H. Sanchez, H. J. McCrea, L. C. Goumnerova, H. W. Song, S. P. Palecek, E. Shusta and D. E. Ingber, Hypoxia-enhanced blood-brain barrier chip recapitulates human barrier function and shuttling of drugs and antibodies, *Nat. Commun.*, 2019, **10**, 2621.

64 B. Noorani, A. Bhalerao, S. Raut, E. Nozohouri, U. Bickel and L. Cucullo, A quasi-physiological microfluidic blood-brain barrier model for brain permeability studies, *Pharmaceutics*, 2021, **13**, 1474.

65 B. Choi, J.-W. Choi, H. Jin, H.-R. Sim, J.-H. Park, T.-E. Park and J. H. Kang, Condensed ECM-based nanofilms on highly permeable PET membranes for robust cell-to-cell communications with improved optical clarity, *Biofabrication*, 2021, **13**, 045020.

66 T. Kurosawa, D. Sako, Y. Tega, Y. Debori, Y. Tomihara, K. Aoyama, Y. Kubo, N. Amano and Y. Deguchi, Construction and functional evaluation of a three-dimensional blood-brain barrier model equipped with human induced pluripotent stem cell-derived brain microvascular endothelial cells, *Pharm. Res.*, 2022, **39**, 1535–1547.

67 S. Fengler, B. Kurkowsky, S. K. Kaushalya, W. Roth, E. Fava and P. Denner, Human iPSC-derived brain endothelial microvessels in a multi-well format enable permeability screens of anti-inflammatory drugs, *Biomaterials*, 2022, **286**, 121525.

68 S. Veszelka, A. Tóth, F. R. Walter, A. E. Tóth, I. Gróf, M. Mészáros, A. Bocsik, É. Hellinger, M. Vastag, G. Rákhely and M. A. Deli, Comparison of a rat primary cell-based blood-brain barrier model with epithelial and brain

endothelial cell lines: gene expression and drug transport, *Front. Mol. Neurosci.*, 2018, **11**, 166.

69 T. Fujimoto, Y. Morofuji, S. Nakagawa, A. Kovac, N. Horie, T. Izumo, M. Niwa, T. Matsuo and W. A. Banks, Comparison of the rate of dedifferentiation with increasing passages among cell sources for an in vitro model of the blood-brain barrier, *J. Neural Transm.*, 2020, **127**, 1117–1124.

70 Y. Uchida, S. Ohtsuki, Y. Katsukura, C. Ikeda, T. Suzuki, J. Kamiie and T. Terasaki, Quantitative targeted absolute proteomics of human blood-brain barrier transporters and receptors, *J. Neurochem.*, 2011, **117**, 333–345.

71 R. Shawahna, Y. Uchida, X. Declèves, S. Ohtsuki, S. Yousif, S. Dauchy, A. Jacob, F. Chassoux, C. Daumas-Duport, P.-O. Couraud, T. Terasaki and J.-M. Scherrmann, Transcriptomic and quantitative proteomic analysis of transporters and drug metabolizing enzymes in freshly isolated human brain microvessels, *Mol. Pharmaceutics*, 2011, **8**, 1332–1341.

72 Y. Uchida, Y. Yagi, M. Takao, M. Tano, M. Umetsu, S. Hirano, T. Usui, M. Tachikawa and T. Terasaki, Comparison of absolute protein abundances of transporters and receptors among blood-brain barriers at different cerebral regions and the blood-spinal cord barrier in humans and rats, *Mol. Pharmaceutics*, 2020, **17**, 2006–2020.

73 H. W. Song, K. L. Foreman, B. D. Gastfriend, J. S. Kuo, S. P. Palecek and E. V. Shusta, Transcriptomic comparison of human and mouse brain microvessels, *Sci. Rep.*, 2020, **10**, 12358.

74 D. Watanabe, S. Nakagawa, Y. Morofuji, A. E. Tóth, M. Vastag, J. Aruga, M. Niwa and M. A. Deli, Characterization of a primate blood-brain barrier co-culture model prepared from primary brain endothelial cells, pericytes and astrocytes, *Pharmaceutics*, 2021, **13**, 1484.

75 E. S. Lippmann, A. Al-Ahmad, S. M. Azarin, S. P. Palecek and E. V. Shusta, A retinoic acid-enhanced, multicellular human blood-brain barrier model derived from stem cell sources, *Sci. Rep.*, 2014, **4**, 4160.

76 A. Appelt-Menzel, A. Cubukova, K. Günther, F. Edenhofer, J. Piontek, G. Krause, T. Stüber, H. Walles, W. Neuhaus and M. Metzger, Establishment of a human blood-brain barrier co-culture model mimicking the neurovascular unit using induced pluri- and multipotent stem cells, *Stem Cell Rep.*, 2017, **8**, 894–906.

77 E. K. Hollmann, A. K. Bailey, A. V. Potharazu, M. D. Neely, A. B. Bowman and E. S. Lippmann, Accelerated differentiation of human induced pluripotent stem cells to blood-brain barrier endothelial cells, *Fluids Barriers CNS*, 2017, **14**, 9.

78 M. J. Stebbins, E. S. Lippmann, M. G. Faubion, R. Daneman, S. P. Palecek and E. V. Shusta, Activation of RARα, RARγ, or RXRα increases barrier tightness in human induced pluripotent stem cell-derived brain endothelial cells, *Biotechnol. J.*, 2018, **13**, 1700093.

79 M. J. Stebbins, B. D. Gastfriend, S. G. Canfield, M. S. Lee, D. Richards, M. G. Faubion, W. J. Li, R. Daneman, S. P. Palecek and E. V. Shusta, Human pluripotent stem cell-derived brain pericyte-like cells induce blood-brain barrier properties, *Sci. Adv.*, 2019, **5**, eaau7375.

80 E. H. Neal, N. A. Marinelli, Y. Shi, P. M. McClatchey, K. M. Balotin, D. R. Gullett, K. A. Hagerla, A. B. Bowman, K. C. Ess, J. P. Wikswo and E. S. Lippmann, A simplified, fully defined differentiation scheme for producing blood-brain barrier endothelial cells from human iPSCs, *Stem Cell Rep.*, 2019, **12**, 1380–1388.

81 T. Qian, S. E. Hernday, X. Bao, W. R. Olson, S. E. Panzer, E. V. Shusta and S. P. Palecek, Directed differentiation of human pluripotent stem cells to podocytes under defined conditions, *Sci. Rep.*, 2019, **9**, 2765.

82 R. M. Linville, J. G. DeStefano, M. B. Sklar, Z. Xu, A. M. Farrell, M. I. Bogorad, C. Chu, P. Walczak, L. Cheng, V. Mahairaki, K. A. Whartenby, P. A. Calabresi and P. C. Searson, Human iPSC-derived blood-brain barrier microvessels: validation of barrier function and endothelial cell behavior, *Biomaterials*, 2019, **190–191**, 24–37.

83 H. Nishihara, B. D. Gastfriend, S. Soldati, S. Perriot, A. Mathias, Y. Sano, F. Shimizu, F. Gosselet, T. Kanda, S. P. Palecek, R. Du Pasquier, E. V. Shusta and B. Engelhardt, Advancing human induced pluripotent stem cell-derived blood-brain barrier models for studying immune cell interactions, *FASEB J.*, 2020, **34**, 16693–16715.

84 B. D. Gastfriend, H. Nishihara, S. G. Canfield, K. L. Foreman, B. Engelhardt, S. P. Palecek and E. V. Shusta, Wnt signaling mediates acquisition of blood-brain barrier properties in naïve endothelium derived from human pluripotent stem cells, *eLife*, 2021, **10**, e70992.

85 M. Heymans, R. Figueiredo, L. Dehouck, D. Francisco, Y. Sano, F. Shimizu, T. Kanda, R. Bruggmann, B. Engelhardt, P. Winter, F. Gosselet and M. Culot, Contribution of brain pericytes in blood-brain barrier formation and maintenance: a transcriptomic study of cocultured human endothelial cells derived from hematopoietic stem cells, *Fluids Barriers CNS*, 2020, **17**, 48.

86 E. L. J. Moya, E. Vandenhaute, E. Rizzi, M. C. Boucau, J. Hachani, N. Maubon, F. Gosselet and M.-P. Dehouck, Miniaturization and automation of a human in vitro blood-brain barrier model for the high-throughput screening of compounds in the early stage of drug discovery, *Pharmaceutics*, 2021, **13**, 892.

87 E. S. Lippmann, S. M. Azarin, S. P. Palecek and E. V. Shusta, Commentary on human pluripotent stem cell-based blood-brain barrier models, *Fluids Barriers CNS*, 2020, **17**, 64.

88 T. M. Lu, S. Houghton, T. Magdeldin, J. G. B. Durán, A. P. Minotti, A. Snead, A. Sproul, D. T. Nguyen, J. Xiang, H. A. Fine, Z. Rosenwaks, L. Studer, S. Rafii, D. Agalliu, D. Redmond and R. Lis, Pluripotent stem cell-derived epithelium misidentified as brain microvascular endothelium requires ETS factors to acquire vascular fate, *Proc. Natl. Acad. Sci. U. S. A.*, 2021, **118**, e2016950118.

89 T. M. Lu, J. G. Barcia Durán, S. Houghton, S. Rafii, D. Redmond and R. Lis, Human induced pluripotent stem cell-derived brain endothelial cells: current controversies, *Front. Physiol.*, 2021, **12**, 642812.

90 M. J. Workman and C. N. Svendsen, Recent advances in human iPSC-derived models of the blood-brain barrier, *Fluids Barriers CNS*, 2020, **17**, 30.

91 F. Roudnicky, B. K. Kim, Y. Lan, R. Schmucki, V. Küppers, K. Christensen, M. Graf, C. Patsch, M. Burcin, C. A. Meyer, P. D. Westenskow and C. A. Cowan, Identification of a combination of transcription factors that synergistically increases endothelial cell barrier resistance, *Sci. Rep.*, 2020, **10**, 3886.

92 R. Paolinelli, M. Corada, L. Ferrarini, K. Devraj, C. Artus, C. J. Czupalla, N. Rudini, L. Maddaluno, E. Papa, B. Engelhardt, P.-O. Couraud, S. Liebner and E. Dejana, Wnt activation of immortalized brain endothelial cells as a tool for generating a standardized model of the blood brain barrier in vitro, *PLoS One*, 2013, **8**, e70233.

93 M. D. Laksitorini, V. Yathindranath, W. Xiong, S. Hombach-Klonisch and D. W. Miller, Modulation of Wnt/β-catenin signaling promotes blood-brain barrier phenotype in cultured brain endothelial cells, *Sci. Rep.*, 2019, **9**, 19718.

94 F. Roudnicky, J. D. Zhang, B. K. Kim, N. J. Pandya, Y. Lan, L. Sach-Peltason, H. Ragelle, P. Strassburger, S. Gruener, M. Lazendic, S. Uhles, F. Revelant, O. Eidam, G. Sturm, V. Kueppers, K. Christensen, L. D. Goldstein, M. Tzouros, B. Banfai, Z. Modrusan, M. Graf, C. Patsch, M. Burcin, C. A. Meyer, P. D. Westenskow and C. A. Cowan, Inducers of the endothelial cell barrier identified through chemogenomic screening in genome-edited hPSC-endothelial cells, *Proc. Natl. Acad. Sci. U. S. A.*, 2020, **117**, 19854–19865.

95 M. Yamashita, H. Aoki, T. Hashita, T. Iwao and T. Matsunaga, Inhibition of transforming growth factor beta signaling pathway promotes differentiation of human induced pluripotent stem cell-derived brain microvascular endothelial-like cells, *Fluids Barriers CNS*, 2020, **17**, 36.

96 P. Garberg, M. Ball, N. Borg, R. Cecchelli, L. Fenart, R. D. Hurst, T. Lindmark, A. Mabondzo, J. E. Nilsson, T. J. Raub, D. Stanimirovic, T. Terasaki, J. O. Oberg and T. Osterberg, In vitro models for the blood-brain barrier, *Toxicol. In Vitro*, 2005, **19**, 299–334.

97 É. Hellinger, S. Veszelka, A. E. Tóth, F. Walter, Á. Kittel, M. L. Bakk, K. Tihanyi, V. Háda, S. Nakagawa, T. D. Duy, M. Niwa, M. A. Deli and M. Vastag, Comparison of brain capillary endothelial cell-based and epithelial (MDCK-MDR1, Caco-2, and VB-Caco-2) cell-based surrogate blood-brain barrier penetration models, *Eur. J. Pharm. Biopharm.*, 2012, **82**, 340–351.

98 B. J. Ballermann, A. Dardik, E. Eng and A. Liu, Shear stress and the endothelium, *Kidney Int. Suppl.*, 1998, **67**, S100–S108.

99 Y. S. Li, J. H. Haga and S. Chien, Molecular basis of the effects of shear stress on vascular endothelial cells, *J. Biomech.*, 2005, **38**, 1949–1971.

100 E. Tzima, M. Irani-Tehrani, W. B. Kiosses, E. Dejana, D. A. Schultz, B. Engelhardt, G. Cao, H. DeLisser and M. A. Schwartz, A mechanosensory complex that mediates the endothelial cell response to fluid shear stress, *Nature*, 2005, **437**, 426–431.

101 L. Koenig, A. P. Ramme, D. Faust, M. Mayer, T. Flötke, A. Gerhartl, A. Brachner, W. Neuhaus, A. Appelt-Menzel, M. Metzger, U. Marx and E. M. Dehne, A human stem cell-derived brain-liver chip for assessing blood-brain-barrier permeation of pharmaceutical drugs, *Cell*, 2022, **11**, 3295.

102 F. Garcia-Polite, J. Martorell, P. Del Rey-Puech, P. Melgar-Lesmes, C. C. O'Brien, J. Roquer, A. Ois, A. Principe, E. R. Edelman and M. Balcells, Pulsatility and high shear stress deteriorate barrier phenotype in brain microvascular endothelium, *J. Cereb. Blood Flow Metab.*, 2017, **37**, 2614–2625.

103 C. Greene, N. Hanley and M. Campbell, Claudin-5: gatekeeper of neurological function, *Fluids Barriers CNS*, 2019, **16**, 3.

104 Y. Hashimoto, C. Greene, A. Munnich and M. Campbell, The CLDN5 gene at the blood-brain barrier in health and disease, *Fluids Barriers CNS*, 2023, **20**, 22.

105 F. R. Walter, A. R. Santa-Maria, M. Mészáros, S. Veszelka, A. Dér and M. A. Deli, Surface charge, glycocalyx, and blood-brain barrier function, *Tissue Barriers*, 2021, **9**, 1904773.

106 R. Santamaría, M. González-Álvarez, R. Delgado, S. Esteban and A. G. Arroyo, Remodeling of the microvasculature: May the blood flow be with you, *Front. Physiol.*, 2020, **11**, 586852.

107 R. M. Linville, M. B. Sklar, G. N. Grifno, R. F. Nerenberg, J. Zhou, R. Ye, J. G. DeStefano, Z. Guo, R. Jha, J. J. Jamieson, N. Zhao and P. C. Searson, Three-dimensional microenvironment regulates gene expression, function, and tight junction dynamics of iPSC-derived blood-brain barrier microvessels, *Fluids Barriers CNS*, 2022, **19**, 87.

108 M. E. Katt, R. M. Linville, L. N. Mayo, Z. S. Xu and P. C. Searson, Functional brain-specific microvessels from iPSC-derived human brain microvascular endothelial cells: the role of matrix composition on monolayer formation, *Fluids Barriers CNS*, 2018, **15**, 7.

109 J.-W. Choi, J. Youn, D. S. Kim and T.-E. Park, Human iPS-derived blood-brain barrier model exhibiting enhanced barrier properties empowered by engineered basement membrane, *Biomaterials*, 2023, **293**, 121983.

110 A. R. Santa-Maria, M. Heymans, F. R. Walter, M. Culot, F. Gosselet, M. A. Deli and W. Neuhaus, Transport studies using blood-brain barrier in vitro models: A critical review and guidelines, in *Physiology, Pharmacology and Pathology of the Blood-Brain Barrier, Handbook of Experimental Pharmacology*, ed. Z. Cader and W. Neuhaus, Springer Nature Switzerland AG, Cham, 2022, ch. 8, vol. 273, pp. 187–204.

111 M. Wadman, FDA no longer has to require animal testing for new drugs, *Science*, 2023, **379**, 127–128.

112 A. Pérez-López, A. I. Torres-Suárez, C. Martín-Sabroso and J. Aparicio-Blanco, An overview of in vitro 3D models of the blood-brain barrier as a tool to predict the in vivo permeability of nanomedicines, *Adv. Drug Delivery Rev.*, 2023, **196**, 114816.

113 BetsholtzLab Database of gene expression in adult mouse brain and lung vascular and perivascular cells, https://

betsholtzlab.org/VascularSingleCells/database.html, (accessed November 2023).

114 M. Vanlandewijck, L. He, M. A. Mäe, J. Andrae, K. Ando, F. Del Gaudio, K. Nahar, T. Lebouvier, B. Laviña, L. Gouveia, Y. Sun, E. Raschperger, M. Räsänen, Y. Zarb, N. Mochizuki, A. Keller, U. Lendahl and C. Betsholtz, A molecular atlas of cell types and zonation in the brain vasculature, *Nature*, 2018, **554**, 475–480.

115 L. He, M. Vanlandewijck, M. A. Mäe, J. Andrae, K. Ando, F. Del Gaudio, K. Nahar, T. Lebouvier, B. Laviña, L. Gouveia, Y. Sun, E. Raschperger, Å. Segerstolpe, J. Liu, S. Gustafsson, M. Räsänen, Y. Zarb, N. Mochizuki, A. Keller, U. Lendahl and C. Betsholtz, Single-cell RNA sequencing of mouse brain and lung vascular and vessel-associated cell types, *Sci. Data*, 2018, **5**, 180160.

116 V. Koo, B. T. Hawkins and Y. Yun, Three-dimensional (3D) tetra-culture brain on chip platform for organophosphate toxicity screening, *Sci. Rep.*, 2018, **8**, 2841.

117 J. Huang, Y. B. Li, C. Charlebois, T. Nguyen, Z. Liu, D. Bloemberg, A. Zafer, E. Baumann, C. Sodja, S. Leclerc, G. Fewell, Q. Liu, B. Prabhakarpandian, S. McComb, D. B. Stanimirovic and A. Jezierski, Application of blood brain barrier models in pre-clinical assessment of glioblastoma-targeting CAR-T based immunotherapies, *Fluids Barriers CNS*, 2022, **19**, 38.

118 B. J. van Meer, H. de Vries, K. S. A. Firth, J. van Weerd, L. G. J. Tertoolen, H. B. J. Karperien, P. Jonkheijm, C. Denning, A. P. IJzerman and C. L. Mummery, Small molecule absorption by PDMS in the context of drug response bioassays, *Biochem. Biophys. Res. Commun.*, 2017, **482**, 323–328.

119 B. Peng, S. Hao, Z. Tong, H. Bai, S. Pan, K. L. Lim, L. Li, N. H. Voelcker and W. Huang, Blood-brain barrier (BBB)-on-a-chip: a promising breakthrough in brain disease research, *Lab Chip*, 2022, **22**, 3579–3602.

120 M. Mir, S. Palma-Florez, A. Lagunas, M. J. López-Martínez and J. Samitier, Biosensors integration in blood-brain barrier-on-a-chip: Emerging platform for monitoring neurodegenerative diseases, *ACS Sens.*, 2022, **7**, 1237–1247.

121 S. Kawakita, K. Mandal, L. Mou, M. M. Mecwan, Y. Zhu, S. Li, S. Sharma, A. L. Hernandez, H. T. Nguyen, S. Maity, N. R. de Barros, A. Nakayama, P. Bandaru, S. Ahadian, H.-J. Kim, R. D. Herculano, E. Holler, V. Jucaud, M. R. Dokmeci and A. Khademhosseini, Organ-on-a-chip models of the blood-brain barrier: Recent advances and future prospects, *Small*, 2022, **18**, e2201401.

122 I. Galea, The blood-brain barrier in systemic infection and inflammation, *Cell. Mol. Immunol.*, 2021, **18**, 2489–2501.

123 F. Takata, S. Nakagawa, J. Matsumoto and S. Dohgu, Blood-brain barrier dysfunction amplifies the development of neuroinflammation: Understanding of cellular events in brain microvascular endothelial cells for prevention and treatment of BBB dysfunction, *Front. Cell. Neurosci.*, 2021, **15**, 661838.

124 T. P. Buzhdygan, B. J. DeOre, A. Baldwin-Leclair, T. A. Bullock, H. M. McGary, J. A. Khan, R. Razmpour, J. F. Hale, P. A. Galie, R. Potula, A. M. Andrews and S. H. Ramirez, The SARS-CoV-2 spike protein alters barrier function in 2D static and 3D microfluidic in-vitro models of the human blood-brain barrier, *Neurobiol. Dis.*, 2020, **146**, 105131.

125 N. A. Boghdeh, K. H. Risner, M. D. Barrera, C. M. Britt, D. K. Schaffer, F. Alem, J. A. Brown, J. P. Wikswo and A. Narayanan, Application of a human blood brain barrier organ-on-a-chip model to evaluate small molecule effectiveness against Venezuelan Equine Encephalitis Virus, *Viruses*, 2022, **14**, 2799.

126 P. Wang, L. Jin, M. Zhang, Y. Wu, Z. Duan, Y. Guo, C. Wang, Y. Guo, W. Chen, Z. Liao, Y. Wang, R. Lai, L. P. Lee and J. Qin, Blood-brain barrier injury and neuroinflammation induced by SARS-CoV-2 in a lung-brain microphysiological system, *Nat. Biomed. Eng.*, 2023, DOI: **10.1038/s41551-023-01054-w**.

127 Y. Tang, F. Soroush, S. Sun, E. Liverani, J. C. Langston, Q. Yang, L. E. Kilpatrick and M. F. Kiani, Protein kinase C-delta inhibition protects blood-brain barrier from sepsis-induced vascular damage, *J. Neuroinflammation*, 2018, **15**, 309.

128 S. Seo, C.-H. Choi, K. S. Yi, S. U. Kim, K. Lee, N. Choi, H. J. Lee, S.-H. Cha and H. N. Kim, An engineered neurovascular unit for modeling neuroinflammation, *Biofabrication*, 2021, **13**, 035039.

129 A. Mehta, A. Desai, D. Rudd, G. Siddiqui, C. J. Nowell, Z. Tong, D. J. Creek, P. Tayalia, P. S. Gandhi and N. H. Voelcker, Bio-mimicking brain vasculature to investigate the role of heterogeneous shear stress in regulating barrier integrity, *Adv. Biol.*, 2022, **6**, e2200152.

130 I. Pediaditakis, K. R. Kodella, D. V. Manatakis, C. Y. Le, S. Barthakur, A. Sorets, A. Gravanis, L. Ewart, L. L. Rubin, E. S. Manolakos, C. D. Hinojosa and K. Karalis, A microengineered Brain-Chip to model neuroinflammation in humans, *iScience*, 2022, **25**, 104813.

131 T. Yang, R. Velagapudi, C. Kong, U. Ko, V. Kumar, P. Brown, N. O. Franklin, X. Zhang, A. I. Caceres, H. Min, A. J. Filiano, R. M. Rodriguiz, W. C. Wetsel, S. Varghese and N. Terrando, Protective effects of omega-3 fatty acids in a blood-brain barrier-on-chip model and on postoperative delirium-like behaviour in mice, *Br. J. Anaesth.*, 2023, **130**, e370–e380.

132 A. L. Nair, L. Groenendijk, R. Overdevest, T. M. Fowke, R. Annida, O. Mocellin, H. E. de Vries and N. R. Wevers, Human BBB-on-a-chip reveals barrier disruption, endothelial inflammation, and T cell migration under neuroinflammatory conditions, *Front. Mol. Neurosci.*, 2023, **16**, 1250123.

133 Y.-L. Zeng, Y. Du, X.-X. Xu, Y.-J. Wang, S.-X. Yu, T. Liu, S. Luo, X.-W. Xiang, W. Liu, Y.-C. Chen, H. Huang, H. Gao, Y. Shen, Y. Luo, C. Bao and Y.-J. Liu, On-chip modeling of physiological and pathological blood-brain barrier microenvironment for studying glial responses to neuroinflammation, *Nano Today*, 2023, **52**, 101947.

134 C. Iadecola, J. Anrather and H. Kamel, Effects of COVID-19 on the nervous system, *Cell*, 2020, **183**, 16–27.e1.

135 M. A. Deli, L. Descamps, M.-P. Dehouck, R. Cecchelli, F. Joó, C. S. Ábrahám and G. Torpier, Exposure of tumor necrosis factor-α to luminal membrane of bovine brain capillary endothelial cells cocultured with astrocytes induces a delayed increase of permeability and cytoplasmic stress fiber formation of actin, *J. Neurosci. Res.*, 1995, **41**, 717–726.

136 R. Rauti, S. Navok, D. Biran, K. Tadmor, Y. Leichtmann-Bardoogo, E. Z. Ron and B. M. Maoz, Insight on bacterial newborn meningitis using a neurovascular-unit-on-a-chip, *Microbiol. Spectrum*, 2023, **11**, e0123323.

137 F. Yu, N. D. S. Kumar, L. C. Foo, S. H. Ng, W. Hunziker and D. Choudhury, A pump-free tricellular blood-brain barrier on-a-chip model to understand barrier property and evaluate drug response, *Biotechnol. Bioeng.*, 2020, **117**, 1127–1136.

138 J.-H. Choi, H. K. Choi and K.-B. Lee, In Situ Detection of Neuroinflammation Using Multicellular 3D Neurovascular-Unit-on-a-Chip, *Adv. Funct. Mater.*, 2023, **33**, 2304382.

139 J. Kealy, C. Greene and M. Campbell, Blood-brain barrier regulation in psychiatric disorders, *Neurosci. Lett.*, 2020, **726**, 133664.